

1 **The glacial isostatic adjustment signal at present-day in northern Europe and the British Isles**
2 **estimated from geodetic observations and geophysical models**

3 Karen M. Simon^{1*}, Riccardo E.M. Riva¹, Marcel Kleinherenbrink¹, Thomas Frederikse^{1,2}

4 ¹Delft University of Technology, Department of Geoscience and Remote Sensing, Stevinweg 1, 2628
5 CN Delft, the Netherlands

6 ²Utrecht University, Institute for Marine and Atmospheric Research, Princetonplein 5, 3584 CC
7 Utrecht, the Netherlands

8 *Corresponding author: +31 15 2788147, k.m.simon@tudelft.nl

9

10 **Abstract**

11 The glacial isostatic adjustment (GIA) signal at present-day is constrained via joint inversion of
12 geodetic observations and GIA models for a region encompassing northern Europe, the British Isles,
13 and the Barents Sea. The constraining data are Global Positioning System (GPS) vertical crustal
14 velocities and GRACE (Gravity Recovery and Climate Experiment) gravity data. When the data are
15 inverted with a set of GIA models, the best-fit model for the vertical motion signal has a χ^2 value of
16 approximately 1 and a maximum *a posteriori* uncertainty of 0.3-0.4 mm/yr. An elastic correction is
17 applied to the vertical land motion rates that accounts for present-day changes to terrestrial hydrology
18 as well as recent mass changes of ice sheets and glaciated regions. Throughout the study area, mass
19 losses from Greenland dominate the elastic vertical signal and combine to give an elastic correction of
20 up to +0.5 mm/yr in central Scandinavia. Neglecting to use an elastic correction may thus introduce a
21 small but persistent bias in model predictions of GIA vertical motion even in central Scandinavia where
22 vertical motion is dominated by GIA due to past glaciations. The predicted gravity signal is generally
23 less well-constrained than the vertical signal, in part due to uncertainties associated with the correction
24 for contemporary ice mass loss in Svalbard and the Russian Arctic. The GRACE-derived gravity trend
25 is corrected for present-day ice mass loss using estimates derived from the ICESat and CryoSat
26 missions, although a difference in magnitude between GRACE-inferred and altimetry-inferred regional
27 mass loss rates suggests the possibility of a non-negligible GIA response here either from millennial-
28 scale or Little Ice Age GIA.

29

30 **1. Introduction**

31 Glacial isostatic adjustment (GIA) is the process by which the Earth's crust and underlying mantle
32 deform in response to surface loading and unloading by large ice sheets and glaciers (e.g., Peltier and
33 Andrews 1976, Wu and Peltier 1982). Glacial isostatic deformation at present-day can include
34 contributions from both recent (annual, decadal) variations to ice cover as well as contributions from
35 millennial-scale variations in ice cover during Pleistocene and Holocene glaciation cycles, although in
36 this study GIA refers to the latter paleo signal, specifically from the last glaciation. Ongoing GIA is
37 usually the dominant present-day deformation signal in formerly glaciated areas (for example, up to
38 approximately 1 cm/yr land uplift around the northwestern Gulf of Bothnia, Lidberg et al. 2010, Kierulf
39 et al. 2014). Outside formerly glaciated regions, the GIA signal from past glaciations often remains
40 large enough to form a significant component of observed present-day deformation and sea-level
41 change rates. Constraint of the GIA signal at present-day is therefore required for accurate separation
42 of the longer time scale and the more recent contributions to present-day land deformation and gravity
43 change (Peltier 1998, Tamisiea 2011). This problem is complicated further by the fact that the GIA
44 signal itself is temporally and spatially complex, therefore making it challenging for models to constrain
45 some of the fundamental parameters relating to both ice cover during past glaciations and the
46 structure of the Earth.

47

48 In Scandinavia, the GIA process has been studied extensively and constrained with data including
49 relative sea level indicators, Global Positioning System (GPS) measurements and satellite gravity data
50 (e.g., Lambeck et al. 1998, Milne et al. 2001, Steffen et al. 2010, see also Steffen and Wu (2011) for a
51 review). While the GIA process in the region of the former Fennoscandian Ice Sheet is probably more
52 extensively studied than anywhere else in the world, GIA in the Barents Sea is by comparison less
53 well understood due in part to the lack of observational evidence left behind by a marine-based ice
54 sheet. Auriac et al. (2016) provide a recent summary of GIA models in the Barents Sea region.
55 Studies have also focussed on the smaller British Isles region, which experiences GIA deformation in
56 response to deglaciation of both the local British Isles Ice Sheet and the larger adjacent
57 Fennoscandian Ice Sheet (Bradley et al. 2011, Kuchar et al. 2012). The ice sheet evolution of the
58 region as a whole was recently summarized by Patton et al. (2017). These studies and many others

59 have provided valuable insight into regional GIA processes. The majority of GIA models are however
60 forward models which can be limited by uncertainties in both the ice sheet model and Earth model.
61 Furthermore, because a best-fit forward GIA model is generally a single Earth-ice model combination,
62 their predictions of GIA deformations are typically provided without uncertainties.

63

64 This paper constrains the GIA signal in northern Europe through the simultaneous inversion of vertical
65 land motion rates from GPS and gravity change rates from GRACE (Gravity Recovery and Climate
66 Experiment). The semi-empirical method also estimates corresponding uncertainties for the preferred
67 model(s) which relative to forward model studies is a notable advantage of semi-empirical or data-
68 driven methodologies. Similar empirical and semi-empirical approaches have been implemented to
69 estimate regional long-term GIA signals in Antarctica (Riva et al. 2009, Gunter et al. 2014), North
70 America (Sasgen et al. 2012, Simon et al. 2017), Alaska (Jin et al. 2016) and Fennoscandia (Hill et al.
71 2010, Müller et al. 2012, Zhao et al. 2012). Here, our methodology is based on that of Hill et al. (2010);
72 relative to their previous work, we update both the GPS and GRACE datasets, incorporate a second
73 model ice sheet history into the *a priori* input, and expand the study area to include regions south and
74 west of Scandinavia, including the British Isles, as well as the Barents Sea to the north. Rather than
75 focus on model parameter estimation, we focus on constraint of the GIA signal at present-day. There
76 are three main goals: i) to model the paleo GIA signal at present-day in a continuous region between
77 Scandinavia and the British Isles, ii) to estimate empirically the uncertainty of the modelled signal, and
78 iii) to assess the importance of applying an elastic correction to the vertical land motion data.

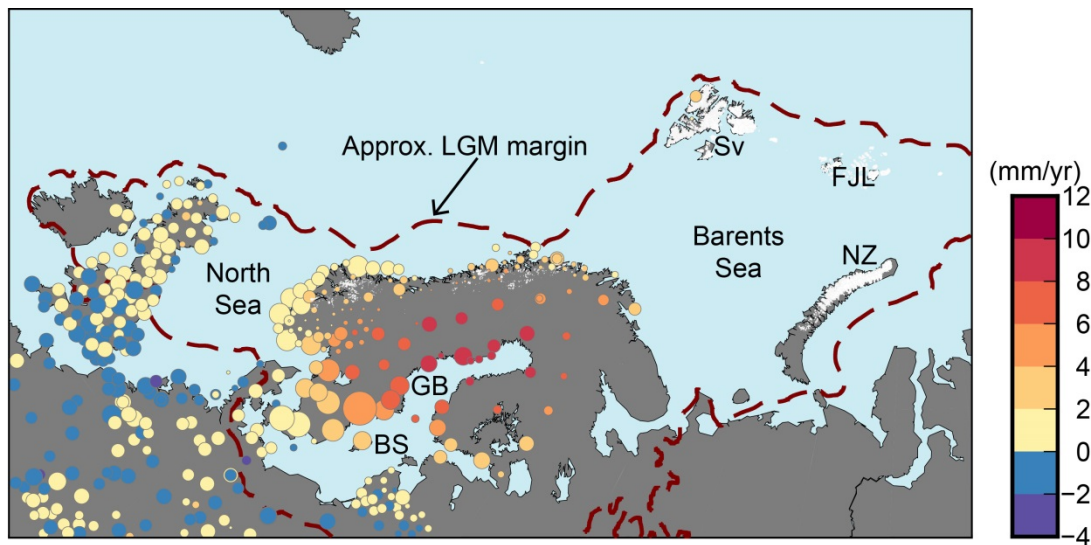
79

80 **2. Model Inputs and Method**

81 **2.1 GPS Data**

82 Rates of vertical land motion measured by GPS are taken from both Kierulf et al. (2014) and the
83 Nevada Geodetic Laboratory (Blewitt et al. 2016) (**Figure 1**). The Kierulf et al. (2014) dataset has
84 relatively dense coverage within the region of the former load centre of the Fennoscandian Ice Sheet
85 (FIS), particularly in Norway, but sparse coverage elsewhere. The data from Blewitt et al. (2016) are
86 thus used for the region outside the former ice sheet margin. The Kierulf et al. (2014) dataset has 150

87 stations with time series lengths of at least 3 years. The data from Blewitt et al. (2016) span 1996-
 88 2016 and have been limited to sites which have at least 10 years of data. To avoid spatial overlap of
 89 sites, the data from Blewitt et al. (2016) have been additionally filtered to include only one site within a
 90 30 km radius (where the site selected within the radius is the one with the largest number of usable
 91 data epochs). The subset of data from Blewitt et al. (2016) has 309 stations. Combined with the Kierulf
 92 et al. (2014) data, there are 459 measurements in total.



93
 94 **Figure 1.** Rates of vertical land motion (mm/yr) for the GPS data used in the inversion, after correction
 95 for elastic effects (Section 2.3). BS – Baltic Sea, FJL – Franz Josef Land, GB – Gulf of Bothnia, NZ –
 96 Novaya Zemlya, Sv – Svalbard, FJL and NZ = Russian Arctic. Dark red dashed line (Hughes et al.
 97 2016) shows the approximate boundary of ice cover at the Last Glacial Maximum (LGM) (ice cover on
 98 Iceland not shown). White shading indicates present-day glaciers. The size of the circles is inversely
 99 proportional to the measurement uncertainty.

100

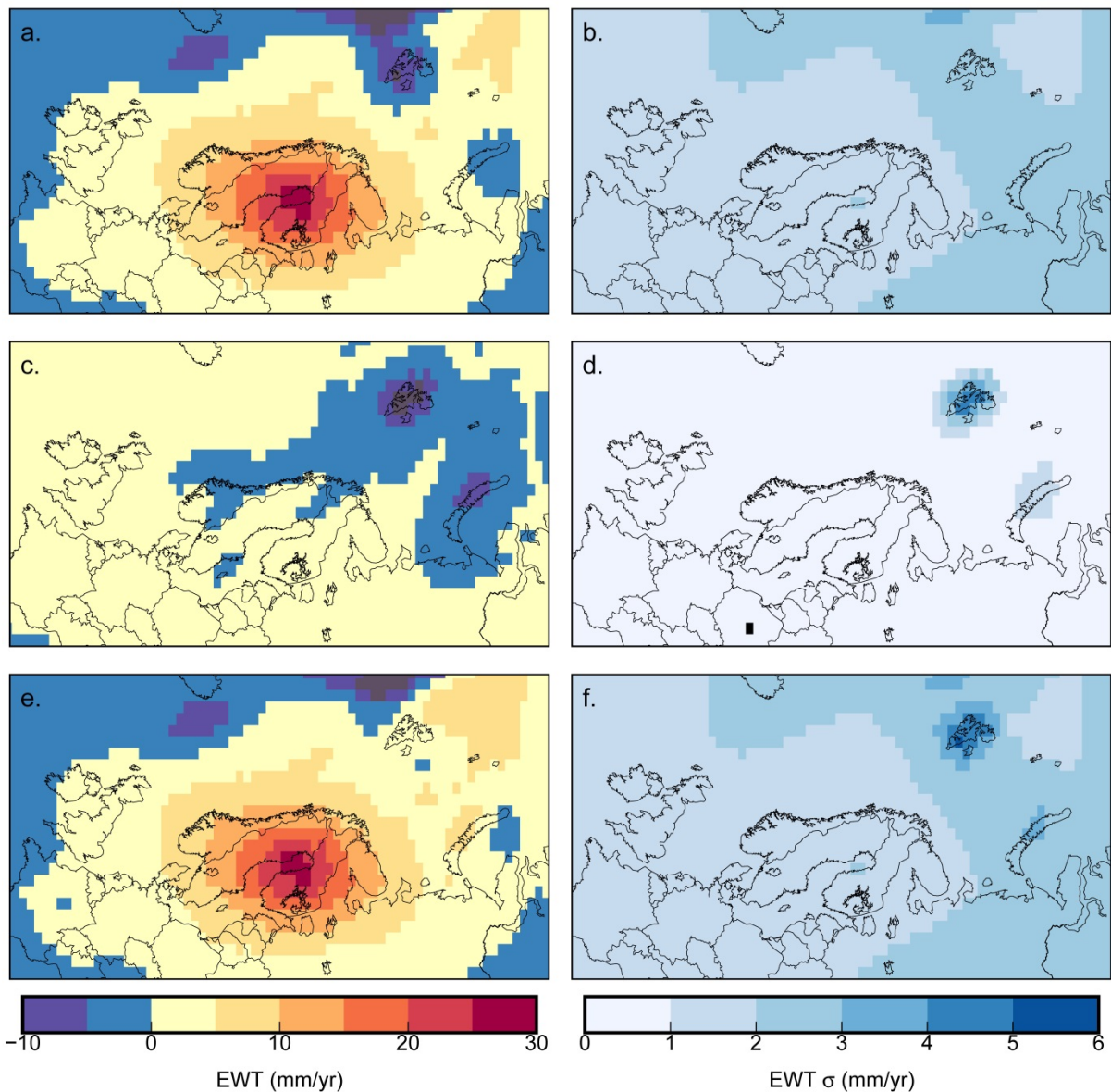
101 As further described in Kierulf et al. (2014), their rates were derived using the GAMIT/GLOBK GPS
 102 analysis software (Herring et al. 2011) and have uncertainties that assume a combination of white
 103 noise and flicker noise, while the data from the Nevada Geodetic Laboratory were calculated using the
 104 MIDAS trend estimator, an algorithm that is less sensitive to discontinuities in GPS time series (Blewitt
 105 et al. 2016). Although the processing technique differs for each dataset, the two datasets are
 106 combined in order to achieve the best possible spatial coverage in the study area. Common sites in
 107 the two datasets compare within the observational uncertainties at all but two of thirty-one sites, and
 108 no apparent bias is observed between the differences at the shared sites (**Figure A1**). Because the
 109 uncertainties are consistently larger for the data from the Nevada Geodetic Laboratory than for the

110 data from Kierulf et al. (2014), we use the common sites to determine an average uncertainty scaling
111 factor (~ 2.25) to apply to the uncertainties in the latter dataset. The scaling avoids significantly biasing
112 the inversion result towards fitting either dataset. Both datasets are aligned in the International
113 Terrestrial Reference Frame 2008 (Altamimi et al. 2011), which is consistent with the CM frame to
114 within ~ 0.2 mm/yr. As described in Section 2.3, an elastic correction is applied that accounts for recent
115 changes in ice sheet and glacier volumes and terrestrial hydrology.

116

117 2.2 GRACE

118 The GRACE data are processed as in Simon et al. (2017). Rates of gravity change for a 10.5 year
119 period from 2004.02-2014.06 are estimated using 113 GRACE Release-05 (RL05) monthly solutions
120 from the University of Texas at Austin Center for Space Research (CSR). The coefficients are
121 truncated at degree and order 96. Part of the GIA signal may also be lost during the filtering,
122 particularly at higher orders; the typical spatial resolution of the signal is ~ 300 km (Siemes et al. 2013).
123 Values estimated from Satellite Laser Ranging (Cheng et al. 2013) replace the C_{20} coefficients.
124 Following Klees et al. (2008), the monthly fields are filtered with a statistically optimal Wiener filter.
125 The optimal filter incorporates the full variance-covariance information of the monthly solutions, and
126 less aggressively filters in regions where signal is stronger. A mass trend is estimated that accounts
127 for bias, annual, and semi-annual variations (**Figure 2**). The signal uncertainty is represented by the
128 full variance-covariance matrix of the trend. Corrections for changes in the terrestrial hydrology cycle
129 and ice mass loss from Svalbard and the Russian Arctic are applied as described in Section 2.3.



130
 131 **Figure 2.** (a) Total gravity change rates measured from GRACE, (c) correction for terrestrial hydrology
 132 changes and present-day ice mass loss (Section 2.3), and (e) final corrected rates. (b,d,f) Same as
 133 (a,c,e) but rates are the 2σ uncertainties associated with the signal. Units are mm/yr change in
 134 equivalent water thickness (EWT).

135

136

137 2.3 Corrections for Terrestrial Hydrology and Present-day Ice Melt

138 Changes in terrestrial hydrology as well as present-day ice mass loss from Greenland, and glaciers
 139 and ice caps in Svalbard, the Russian Arctic, and Scandinavia may form a significant contribution to
 140 the total measured gravity change and vertical motion rates within the study area.

141

142 GRACE

143 In the continental region and south of approximately 71.5° N latitude, hydrological changes are the
144 sum of dam retention values (Chao et al. 2008) and anthropogenic groundwater depletion estimated
145 with the model PCR-GLOBWB (Wada et al. 2014). The trend is computed for 2004-2014 from 11
146 annual means on a 2° × 2° grid, consistent with the resolution of the GRACE data. In glaciated regions
147 (Scandinavia, Svalbard and the Russian Arctic), the hydrology model is not used to correct the input
148 rates. Rather, it is assumed that present-day estimates of regional ice melt derived from altimetry
149 observations should more accurately capture the dominant hydrological signals that would be
150 modelled by PCR-GLOBWB. The corrections for mass loss from the glaciers are also filtered to be
151 consistent with the spatial resolution of the GRACE data. The total correction for hydrology and glacial
152 mass loss is shown in **Figure 2c**, the individual contributions are shown in **Figure A2**.

153

154 Estimates of present-day mass changes in Scandinavia, the Russian Arctic, and Svalbard are
155 summarized in **Table 1** for various studies, and vary considerably depending on estimation method
156 and time period. Ice mass loss in Scandinavia originates from glaciers in western Norway and is
157 consistently small with estimated rates between -1.2 to -2 Gt/yr. Here, we apply a mass loss rate of -
158 1.3 Gt/yr, determined by glaciological modelling (Marzeion et al. 2012, 2015).

159

160 In the Russian Arctic, glaciological estimates of mass change are consistent within uncertainties for
161 the different time periods and suggest mass change between -21.0 to -24.7 Gt/yr. These rates are
162 approximately twice those estimated by the ICESat and CryoSat missions, which estimate mass
163 changes in this region of between -10.5 to -14.9 Gt/yr, with a small acceleration observed after 2010
164 (Wouters, *pers. comm.*, 2016). The smallest net mass change estimate for the Russian Arctic comes
165 from GRACE, with -5.7 Gt/yr mass change observed between 2003-2013 (Schrama et al. 2014).

166

167 In Svalbard, estimated mass change rates are more discrepant. Again, glaciological estimates are the
168 largest, but two estimates of -42.0 Gt/yr and -17.0 Gt/yr between 2003-2009 are not consistent within

169 uncertainties and differ in magnitude by more than a factor of 2. Laser and radar altimetry estimates
 170 are smaller, and suggest a clear acceleration in mass loss since 2010 (-4.6 Gt/yr between 2003-2009
 171 and -16.5 Gt/yr between 2010-2014, Wouters, *pers. comm.*, 2016). As with the Russian Arctic,
 172 GRACE is the estimation technique that records the smallest net mass change, with -4.0 Gt/yr
 173 estimated in Svalbard between 2003-2013 (Schrama et al. 2014).

174

Study/Source	Svalbard (Gt/yr)	Russian Arctic (Gt/yr)	Scandinavia (Gt/yr)
2003-2009			
Marzeion et al. (2015) (2003-2009)	-42.0 ± 3.2 (gl)	-22.9 ± 4.7 (gl)	-1.2 ± 0.2 (gl)
Gardner et al. (2013) (2003-2009)	-17.0 ± 6.0 (gl) -5.0 ± 2.0 (I, G)	-21.0 ± 13.0 (gl) -11.0 ± 4.0 (I, G)	-2.0 ± 0.0 (gl)
Wouters (2016) (2003-2009)	-4.6 ± 1.2 (I)	-10.5 ± 1.3 (I)	-
2010-2014			
Wouters (2016) (2010-2014)	-16.5 ± 1.6 (C)	-14.9 ± 1.2 (C)	-
≥10 years time period			
Marzeion et al. (2015) (2004-2013)	-39.8 ± 2.2 (gl)	-24.7 ± 3.0 (gl)	-1.3 ± 0.1 (gl)
Average Wouters (2016) (2003-2014)	-10.6 ± 2.0 (I, C)	-12.7 ± 1.8 (I, C)	-
Schrama et al. (2014) (2003-2013)	-4.0 ± 0.7 (G)	-5.7 ± 0.9 (G)	+1.3 ± 0.9 (G)
This study	-10.6 ± 2.0 (I, C)	-12.7 ± 1.8 (I, C)	-1.3 ± 0.1 (gl)
This study, with scaling	-2.7 ± 2.0 (I, C)	-2.5 ± 1.8 (I, C)	-1.3 ± 0.1 (gl)*

175 **Table 1.** Estimates of present-day mass change for Svalbard, the Russian Arctic, and Scandinavia for
 176 different time periods and from different sources. Letters in parentheses indicate estimation method; gl
 177 - glaciological, I - IceSat, G - GRACE, C - CryoSat. All rates are in Gt/yr. *Not scaled.

178

179 GRACE measures total mass changes (solid Earth plus cryosphere), and thus a correction for one
 180 needs to be applied in order to isolate the other. While the glaciological values and the altimetry

181 estimates (which are corrected for crustal uplift due to GIA) are both intended to represent changes to
182 the cryosphere, the differing mass change estimates among measurement techniques for the Russian
183 Arctic and Svalbard raise the question of which value to use when applying a correction to the total
184 GRACE trend shown in **Figure 2a**. Relative to GRACE, the glaciological and altimetry methods both
185 consistently infer larger mass losses, suggesting that GRACE contains a significant mass gain signal
186 from the solid Earth, either from glacial isostatic adjustment from the last glaciation, or from the Little
187 Ice Age (LIA). For both Svalbard and the Russian Arctic, we choose to apply an estimate that
188 averages the ICESat and CryoSat estimates over the years 2003-2014 (**Table 1**). Subtracting these
189 averaged rates from the total GRACE estimates for a similar time period (2003-2013, Schrama et al.
190 2014, **Table 1**), infers a reasonably consistent total solid Earth or GIA signal of +6.6-7 Gt/yr in the
191 region.

192

193 However, applying the averaged ice melt corrections to Svalbard and the Russian Arctic creates a
194 large mass gain signal over these two areas and a relatively smaller signal in the central Barents Sea;
195 this pattern is generally inconsistent with ice coverage in the Barents Sea region suggested by several
196 different Pleistocene ice sheet reconstructions (Auriac et al. 2016), and therefore inconsistent with the
197 paleo GIA signal that the input signal should represent. Possible explanations for this inconsistency
198 are: i) models of LGM ice cover in the region require thicker ice over Svalbard and the Russian Arctic
199 than in the Barents Sea, ii) there is a large Little Ice Age GIA signal over these two regions, and/or iii)
200 the Wiener filter applied to the GRACE data too aggressively filters signal in these small regions. The
201 first explanation is unlikely because glacial margin chronology suggests that Svalbard and the Russian
202 Arctic were located on or near the margin of the Barents Ice Sheet where ice cover would have been
203 thinnest. To counteract the effect of either of the latter two explanations (LIA rebound or signal loss in
204 GRACE), we apply ad-hoc scaling factors of 0.25 and 0.2 to the ice mass loss estimates in Svalbard
205 and the Russian Arctic (**Table 1**), so that their removal from the total GRACE signal results in a spatial
206 pattern in the residual (i.e., paleo GIA) signal that is approximately consistent with thicker LGM ice
207 cover over the Barents Sea than around its margins (**Figure 2e**). Such a scaling factor approach is
208 certainly not ideal, but serves to provide a GRACE input signal in the Barents Sea region that has a
209 spatial pattern broadly consistent with expectations of the paleo GIA response to loading and
210 unloading from the Barents Ice Sheet.

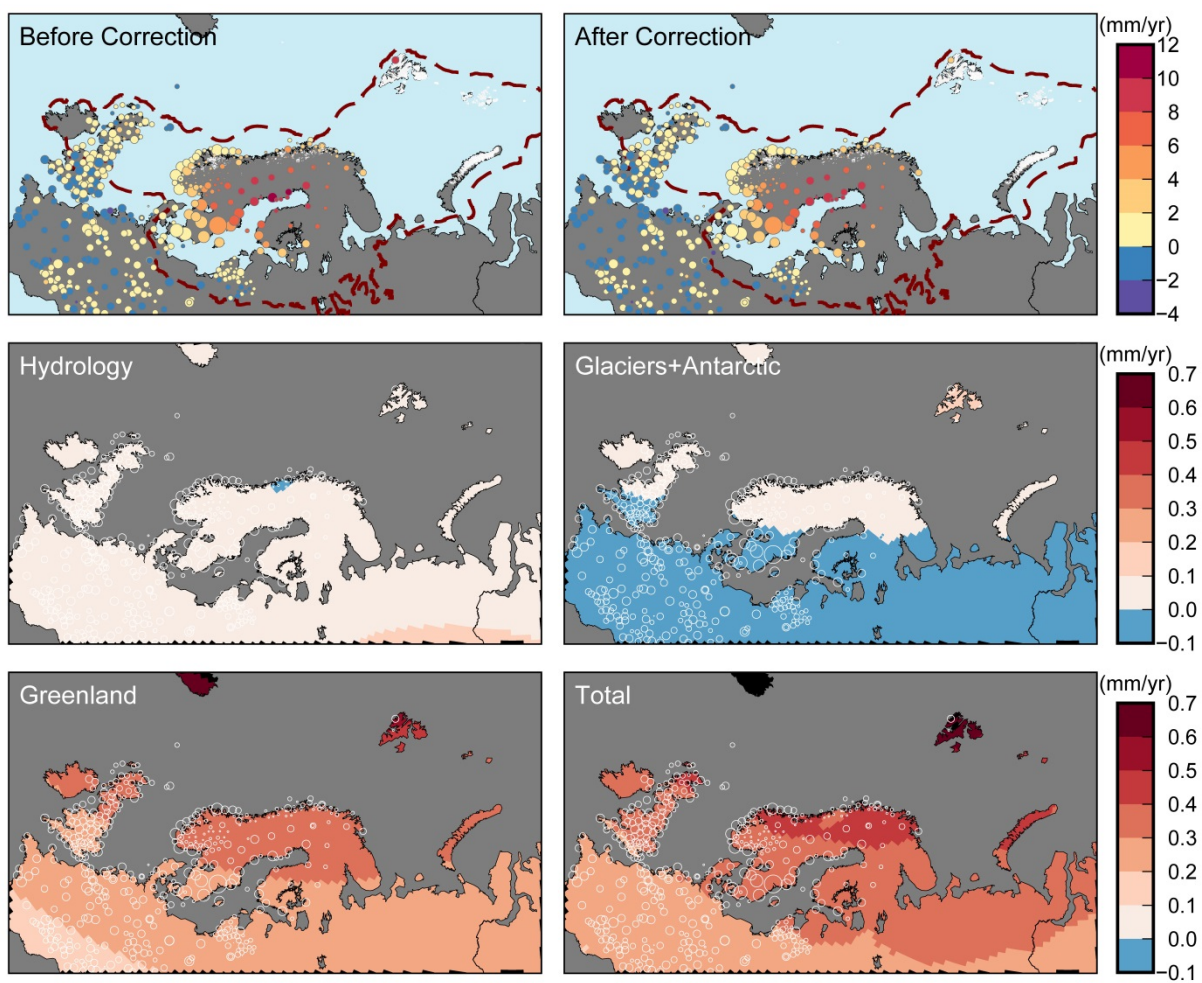
211 GPS

212 Vertical land motion rates may likewise be affected by present-day ice mass loss and the terrestrial
213 hydrology cycle. As with the GRACE data, the GPS data are corrected for changes to terrestrial
214 hydrology south of 71.5° N latitude using predictions from the PCR-GLOBWB model, although here,
215 the hydrology trend has been estimated from 1993-2014 to be more consistent with the length of the
216 GPS time series. North of 71.5° N latitude, the same scaled corrections derived from ICESat and
217 CryoSat are applied for present-day ice mass changes in Svalbard and the Russian Arctic.

218 Throughout the study area, the GPS measurements are also corrected for additional elastic vertical
219 motion from mass loss of the Greenland Ice Sheet, the Antarctic Ice Sheet and glaciers and ice caps
220 in northern Canada. Mass loss of the Greenland Ice Sheet is estimated from 1993-2014 using surface
221 mass balance estimates from RACMO2.3 (Noël et al. 2015) and ice discharge with a constant
222 acceleration of 6.6 Gt/yr² (van den Broeke et al. 2016). Mass loss of the Antarctic Ice Sheet is also
223 estimated from 1993-2014 using RACMO2.3p1 and assuming a constant acceleration in ice discharge
224 of 2 Gt/yr² (van Wessem et al. 2016). The scenarios for both Greenland and Antarctica are consistent
225 with the mass balance estimates from Shepherd et al. (2012). For the Canadian Arctic, a constant
226 mass loss rate of 60 Gt/yr is used (Gardner et al. 2013). All trends and accelerations are calculated
227 with annual time steps. The vertical elastic response is computed in the CM frame using a pseudo-
228 spectral approach up to degree and order 360 and includes the effect of rotational feedback. The
229 respective loads in each year are applied to a spherically symmetric Earth model (e.g., Farrell 1972)
230 using elastic Earth parameters from the Preliminary Reference Earth Model (Dziewonski and
231 Anderson 1981). Linear trends in the calculated vertical motion time series are then estimated by least
232 squares over the years 1993-2014 for each region, and finally summed to yield the total elastic
233 response. All signals combine to yield a total net uplift of approximately 0.2-0.5 mm/yr throughout most
234 of the study area, with Greenland mass loss providing the largest contribution (**Figure 3**). The
235 additional uncertainties are also computed and added in quadrature to the measurement uncertainties;
236 correction of the GPS data for non-GIA signals adds < ±0.05 mm/yr uncertainty in most of the study
237 area and ~±0.1 mm/yr in Svalbard (**Figure 3**).

238

239 Finally, in addition to present-day ice mass loss signals, a correction of 4.33 ± 0.40 mm/yr is removed
 240 from the vertical motion rates for the two GPS sites on Svalbard (NYAL and LYRS). This value is an
 241 average of 3 scenarios from Mémin et al. (2014) which estimate the vertical land motion at Ny-Ålesund
 242 due to Pleistocene and Little Ice Age GIA signals; their estimates range from 3.31-4.95 mm/yr; thus
 243 the averaged correction of 4.33 mm/yr that is applied assumes that the signal from Pleistocene GIA is
 244 small and that most residual land motion here is from LIA rebound. After correction for present-day ice
 245 mass changes and approximated LIA uplift, the residual (inferred paleo GIA) vertical uplift rates at
 246 NYAL and LYRS are 2.64 ± 0.80 and 1.10 ± 2.64 mm/yr, respectively.



247
 248 **Figure 3.** GPS-measured rates of vertical land motion before and after the applied elastic correction
 249 (top left and right). An elastic correction is computed for mass loss from Greenland, the West Antarctic
 250 Ice Sheet (WAIS), glaciers and ice caps in northern Canada, Svalbard and the Russian Arctic, and
 251 loading from the terrestrial hydrology cycle. Sites on Svalbard are additionally corrected for LIA uplift
 252 as discussed in the text.

253

254

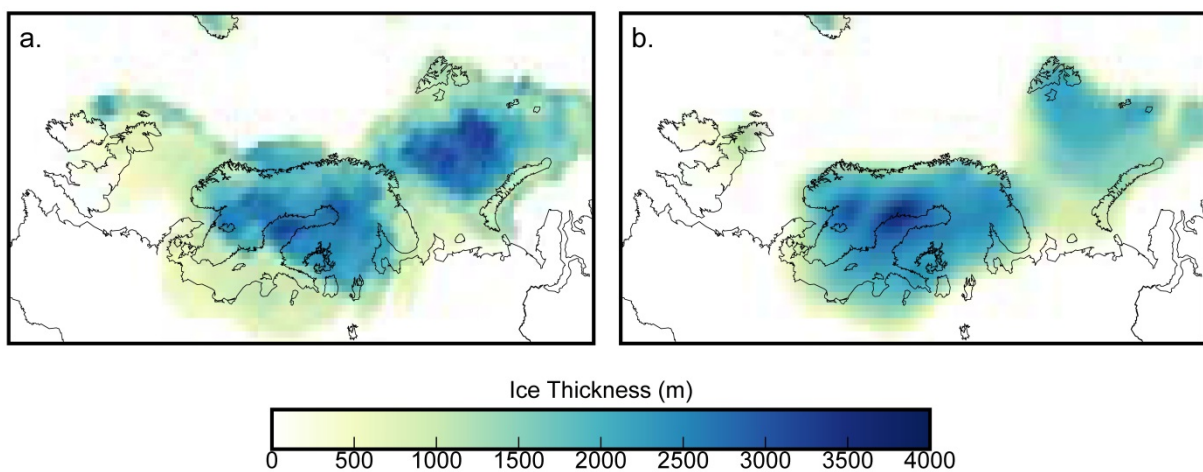
255 2.4 *A Priori* Model Information

256 The prior model covariance matrix contains predictions from a set of forward GIA models that varies
257 ice sheet history and mantle viscosity and is constructed as described in Hill et al. (2010) and Simon
258 et al. (2017). Here, two different ice sheet histories are coupled to a suite of three-layer Earth models
259 with an elastic lithosphere and varying upper and lower mantle viscosities.

260

261 The first ice sheet model is the global ICE-5G model (Peltier 2004). We later compare the data-driven
262 predictions to the more recent ICE-6G forward model (Peltier et al. 2015) (Section 3.3); without ICE-
263 6G in the *a priori* information, the compared predictions are independent to the extent possible. In the
264 second ice sheet model, the glacial history over Fennoscandia and the British Isles is described by the
265 model(s) from the Australian National University (ANU, Lambeck et al. 2010). This second version of
266 the ice sheet model contains ICE-5G coverage over Greenland and Antarctica and the model of North
267 American coverage presented in Simon et al. (2015, 2016). Tests indicate that varying the ice sheet
268 history over North America has little impact on the predictions in Fennoscandia, although this variation
269 is useful for studies that wish to expand the study area outside of the current study area. Relative to
270 ICE-5G, LGM ice cover in the ANU model is thinner over the Barents Sea, thicker over Svalbard and
271 Scotland, and discontinuous between Scandinavia and the British Isles (**Figure 4**).

272



273

274 **Figure 4.** Last glacial maximum (LGM) ice cover in Scandinavia, the Barents Sea and the British Isles
275 from ICE-5G (a) and the ANU model (b).

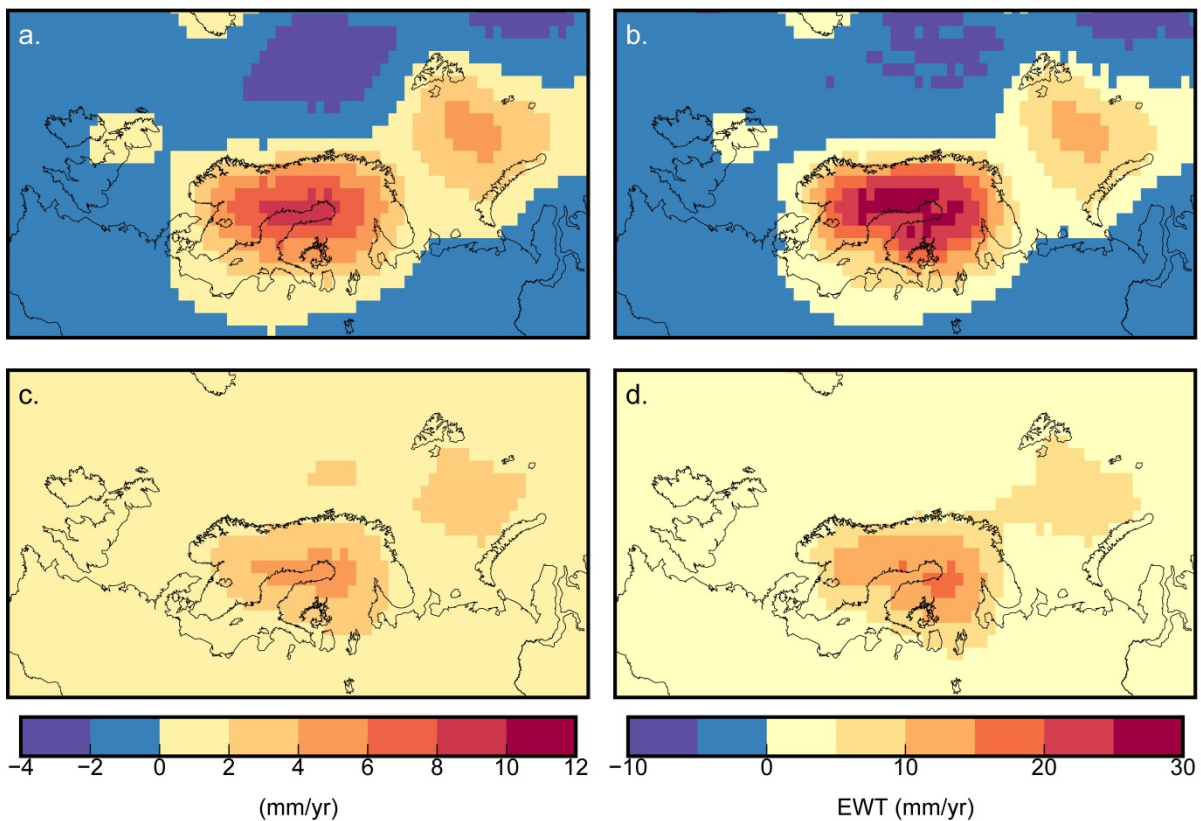
276

277 Previous GIA modelling studies can be used to infer a range of reasonable Earth model parameters
278 for the *a priori* model set. Steffen and Wu (2011) reviewed the results of several GIA modelling studies
279 of the Fennoscandian region and indicated that these analyses suggest regional upper mantle
280 viscosities of between $0.1 - 1 \times 10^{21}$ Pa s and lower mantle viscosities approximately one to two
281 orders of magnitude larger (so $1 - 100 \times 10^{21}$ Pa s). They further indicated that lithospheric thickness
282 in Fennoscandia is likely variable with values ranging from 80 – 200 km (Steffen and Wu 2011).
283 Studies that have followed Steffen and Wu's (2011) review infer slightly narrower ranges for Earth
284 parameters in Fennoscandia. Depending on the ice sheet history and data constraints, the studies of
285 Zhao et al. (2012), Kierulf et al. (2014), Schmidt et al. (2014) and Patton et al. (2017) infer values of
286 upper mantle viscosity, lower mantle viscosity, and lithospheric thickness that may range from (or lie
287 within) $0.34 - 3 \times 10^{21}$ Pa s, $3 - 50 \times 10^{21}$ Pa s, and 93 – 160 km, respectively. In the British Isles,
288 Kuchar et al. (2012) infer upper and lower mantle viscosities of 3×10^{21} Pa s and 2×10^{22} Pa s
289 respectively, consistent with the values inferred by Bradley et al. (2011). Both studies find a best fit
290 lithospheric thickness of 71 km in this region. In the Barents Sea region, Auriac et al. (2016)
291 summarize the performance of six ice sheet models; the four best-fitting models infer respective upper
292 and lower mantle viscosities of $0.2 - 2 \times 10^{21}$ Pa s and $1 - 50 \times 10^{21}$ Pa s and lithospheric thicknesses
293 of 71 – 120 km. Both the studies of Root et al. (2015) and Patton et al. (2017) infer Earth parameters
294 for this region that are within the ranges given by Auriac et al. (2016).

295

296 Considering these three regions as a whole gives minimum to maximum ranges for upper and lower
297 mantle viscosity and lithospheric thickness of $0.2 - 3 \times 10^{21}$ Pa s, $3 - 50 \times 10^{21}$ Pa s and 71 – 160 km.
298 These mantle viscosity ranges are consistent with those used in our prior model set, which range from
299 $0.2 - 2 \times 10^{21}$ Pa s and $1 - 60 \times 10^{21}$ Pa s in the upper and lower mantle. The prior model set uses an
300 elastic lithospheric thickness of 90 km, although future analyses could benefit from use of a wider
301 range of thicknesses. With regard to the mantle viscosities, we note that both the ICE-5G and ANU ice
302 sheet models were not developed independently from a description of mantle viscosity. While the
303 coupling of a set of differing Earth models to a 'tuned' ice sheet history may introduce artificially high
304 variances, this concern may be countered by considering that the variances in such an *a priori* Earth-

305 ice model set could almost certainly be made larger if any combination of 3D Earth structure, non-
306 linear mantle rheology or glaciological and climatological constraints were additionally incorporated. A
307 full covariance matrix is generated that relates the variances of each model prediction relative to the
308 suite's average. All models are represented at spherical harmonic degree and order 256. The average
309 response and uncertainties of the *a priori* set is shown in **Figure 5**.



310
311 **Figure 5.** Averaged *a priori* rates of the Earth-ice model set. (a, c) Vertical rates and uncertainties. (b,
312 d) Gravity change rates and uncertainties in units of equivalent water thickness (EWT) change.

313

314 2.5 Method

315 The least-squares adjustment method is based on the methodology of Hill et al. (2010) and extended
316 by Simon et al. (2017). The method simultaneously inverts the data constraints (GPS, GRACE or
317 both) with the *a priori* GIA model information and minimizes the misfit to both input types. As in Simon
318 et al. (2017), variance component estimation (VCE) is also used to weight the input uncertainties. The
319 prior models are combined with the data in three scenarios: inversion with the GPS data alone (D1),
320 inversion with the GRACE data alone (D2), and inversion with both datasets (D3).

321

322 3. Results and Discussion

323 3.1 Prediction of Vertical Motion and Gravity Change

324 *Vertical Motion*

325 The predicted GIA response and uncertainties for the D1-D3 scenarios are shown for vertical land
326 motion (**Figure 6**). The incorporation of the GPS data in scenarios D1 and D3 leads to a similar
327 pattern of regional uplift although relative to D1, the D3 scenario predicts slightly lower rates of uplift
328 over the northern British Isles and in the Barents Sea. D1 and D3 have respective peak uplift rates of
329 9.8 and 9.2 mm/yr. When only the gravity data are inverted in the D2 scenario, the region of uplift is
330 broader and the peak uplift rate is smaller at 7.1 mm/yr. In all cases, the peak uplift is centred over the
331 northwestern region of the Gulf of Bothnia. The peak (1σ) uncertainty rates are ± 0.36 , ± 0.43 and ± 0.28
332 mm/yr for the D1-D3 cases. Similar to the results of Simon et al. (2017), the predicted uncertainties
333 are largest where the signal is largest (around the Gulf of Bothnia) and/or the data coverage is
334 sparsest and most poorly constrained (around the Barents Sea). In Finland, for example, the relatively
335 large signal and the relatively sparse data coverage combine to create a region of larger uncertainty
336 than in surrounding areas. The inclusion of VCE does not significantly impact the signal prediction but
337 in general somewhat increases the estimated *a posteriori* model uncertainty; the weighting factors
338 determined by VCE are shown in **Table 2**. In model D1, both the uncertainties of the vertical velocities
339 and the prior model set are slightly reduced. In model D3, the uncertainties of the vertical velocities
340 are basically unscaled (increased by a factor of 1.02) whereas the covariances of the prior model set
341 are reduced by a factor of 0.64 (note however that the original covariances of the prior model set are
342 still generally larger than those of the vertical data, at least in the region of the former load centre).

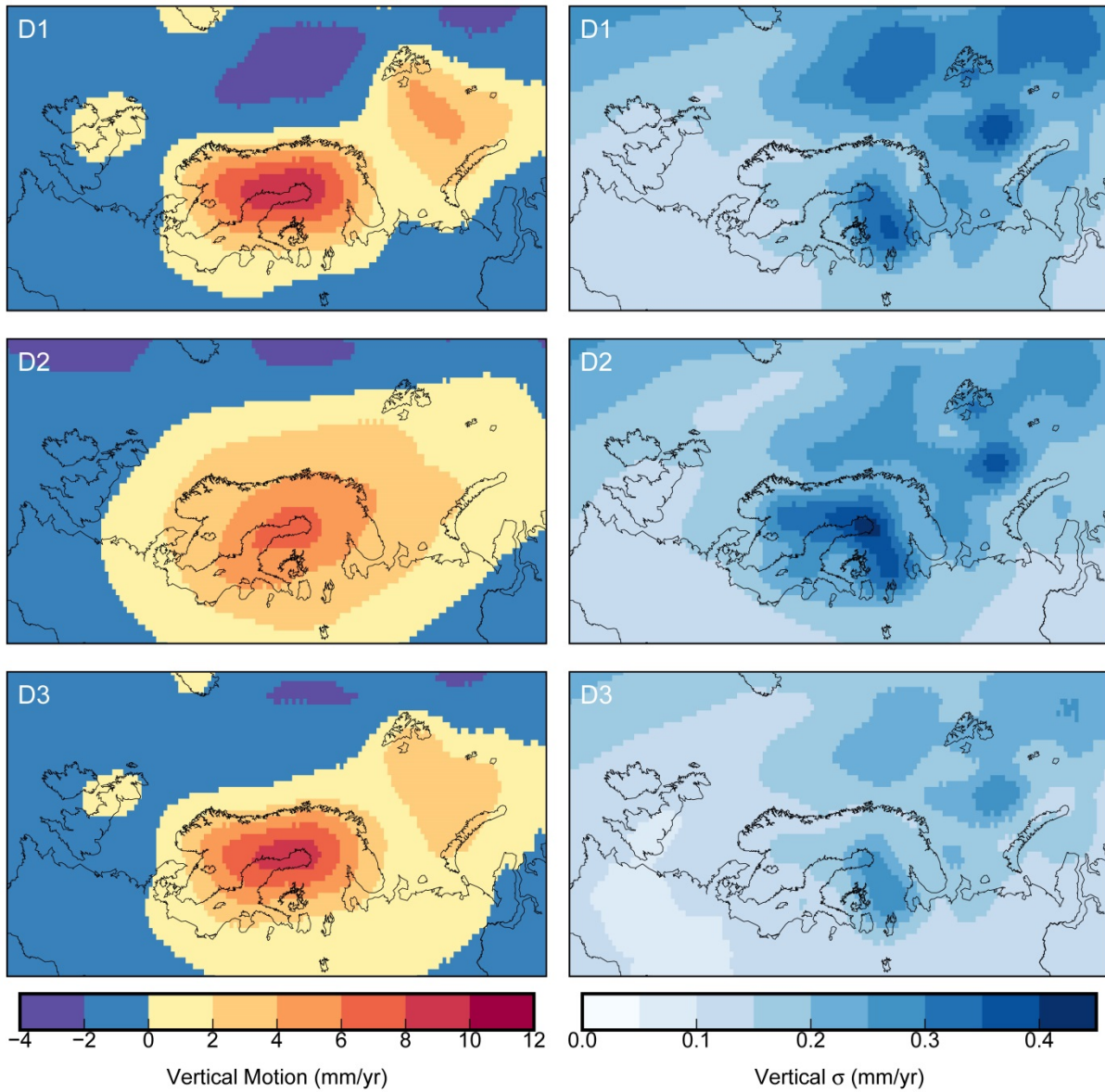
343

344 *Gravity Change*

345 The predicted gravity change rates for D1-D3 are comparable to the predicted vertical motion rates in
346 both the spatial pattern and relative magnitude (not shown). The peak mass change rates are again
347 centred over the northern Gulf of Bothnia, and are 33.7, 24.3, and 32.3 mm/yr of equivalent water
348 thickness change for the D1-D3 scenarios. The peak associated 1σ uncertainties are ± 1.59 , ± 1.59

349 and ± 1.22 mm/yr EWT. In both the D2 and D3 models, the uncertainties of the GRACE data are
350 increased by the VCE analysis (**Table 2**).

351



352
353 **Figure 6.** Prediction of present-day vertical land motion (left) and uncertainties (right) due to long-term
354 GIA for the D1-D3 scenarios.

355

356

357

358

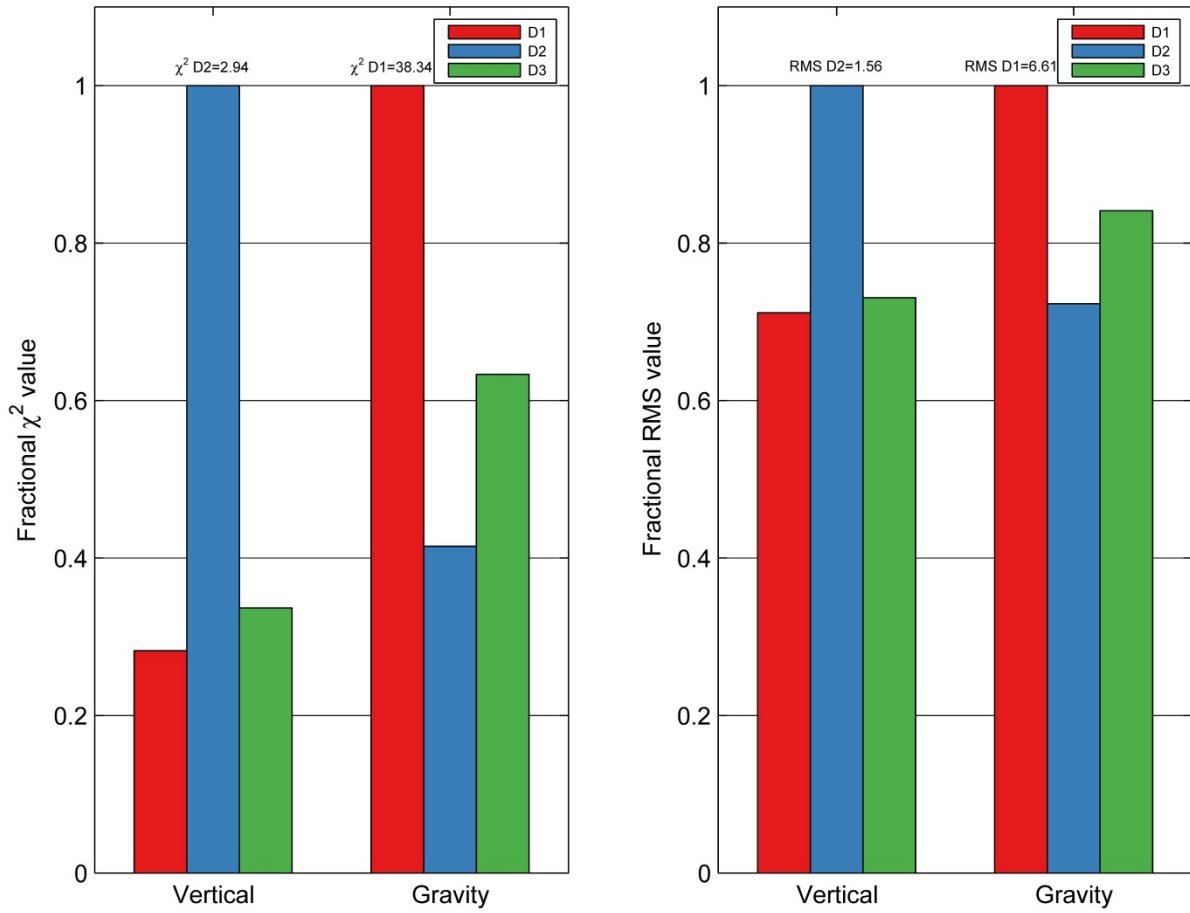
Data Incorporated	σ^2 Squared Value			Ratios	
	σ_1^2 (Vertical)	σ_2^2 (Gravity)	σ_μ^2 (Prior)	σ_1^2/σ_2^2	$\sigma_1^2/\sigma_\mu^2, \sigma_2^2/\sigma_\mu^2$
D1: Vertical only	0.85	-	0.94	-	0.90, -
D2: Gravity only	-	13.51	0.61	-	-, 22.15
D3: Vertical+Gravity	1.02	20.55	0.64	0.05	1.59, 32.11

359 **Table 2.** Results of the variance component analysis. σ_1^2 and σ_2^2 are the variance factors applied to the
360 vertical motion data (dataset 1) and gravity change data (dataset 2), respectively, and σ_μ^2 is the
361 variance factor applied to the prior information. The ratios describe how each input covariance matrix
362 is weighted relative to the other(s).

363

364 3.2 Misfit Values and Residuals

365 For both χ^2 and RMS values, the D1 model provides the best fit to the vertical data, the D2 model
366 provides the best fit to the gravity data, and the D3 model provides the best fit overall (**Figure 7**). The
367 χ^2 values of the vertical prediction for both D1 and D3 are approximately equal to 1. The χ^2 values for
368 the gravity data are relatively large with the smallest value of 15.9 obtained for the D2 model. Scaling
369 the gravity data uncertainties by the VCE-determined scaling factors in **Table 2** reduces the overall χ^2
370 values for the gravity prediction to approximately 1.2 for the D2 and D3 models. However, the
371 statistical fit of the models to the gravity data remains generally worse than the fit to the vertical motion
372 data.



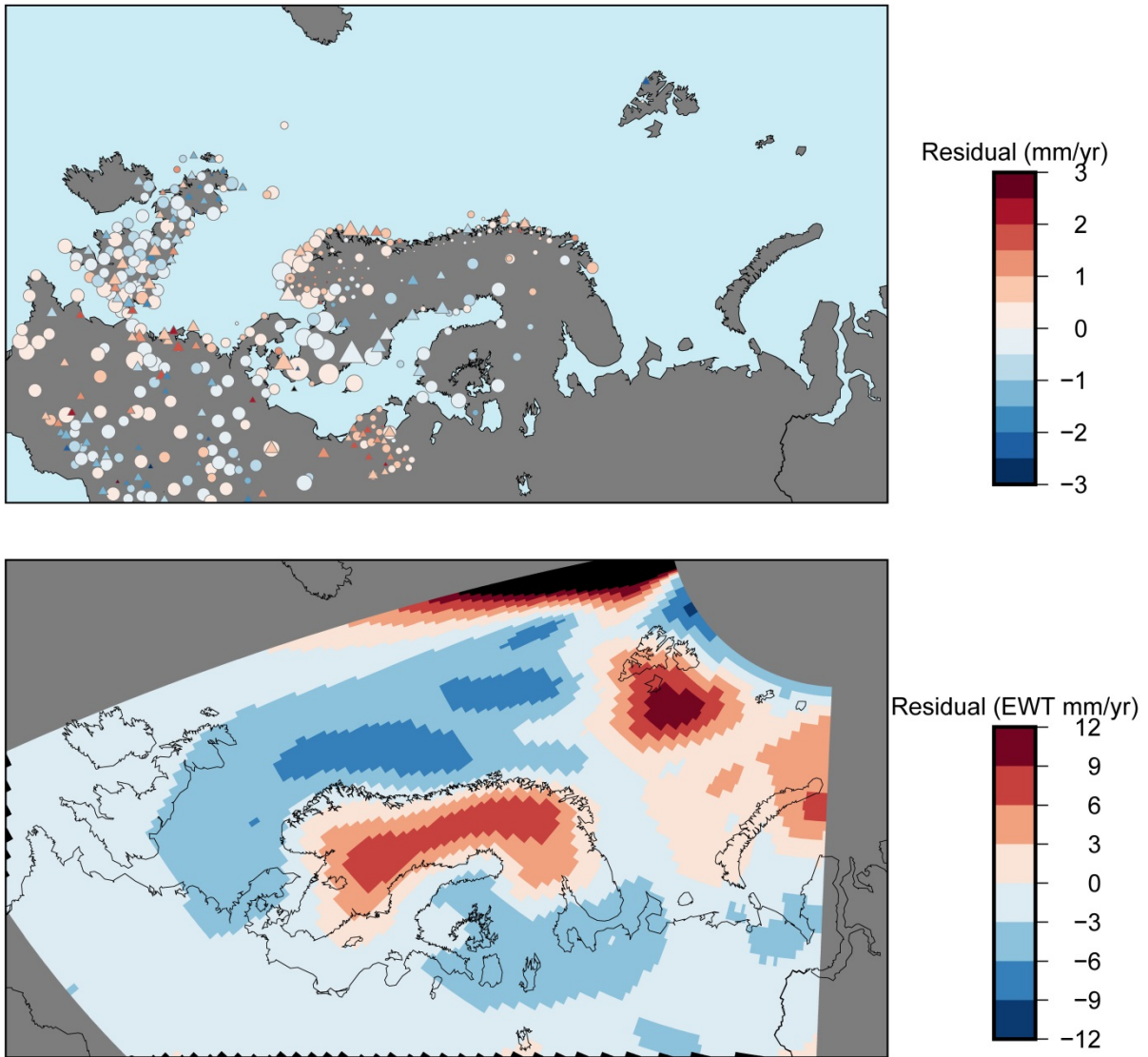
373

374 **Figure 7.** Fractional χ^2 and RMS values for each of the D1-D3 models. Fractional values are
 375 determined relative to the value of the worst fitting model for both the vertical motion and gravity
 376 change predictions (i.e., fractional χ^2 values of the vertical motion prediction are relative to D2 for
 377 which $\chi^2 = 2.94$). χ^2 values are not VCE-scaled; see **Figure 8** for all χ^2 values including with and
 378 without VCE scaling, where applicable.

379

380 **Figures 8-9** summarize the spatial residuals for the best-fit D3 model and the binned residuals for all
 381 models. The vertical motion residuals are unbiased and generally small. Regionally, the D3 model
 382 underpredicts vertical motion in Scotland and conversely overpredicts vertical motion along parts of
 383 the southern Norwegian coast and the Netherlands. The gravity residuals for D3 are relatively low for
 384 much of the study area, although there is noticeable overprediction in central Scandinavia and in the
 385 Barents Sea.

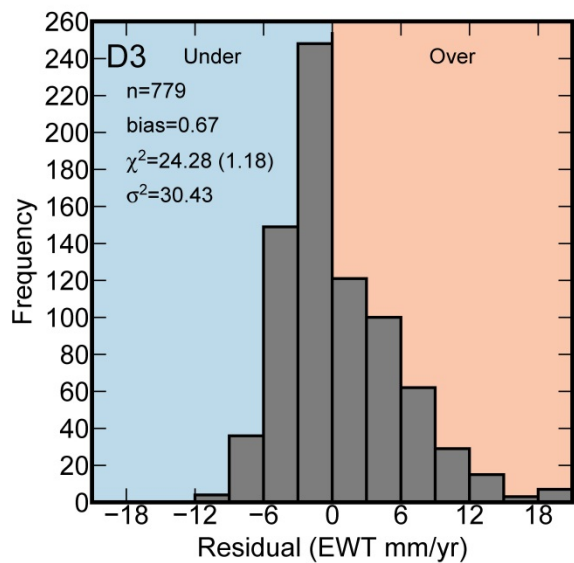
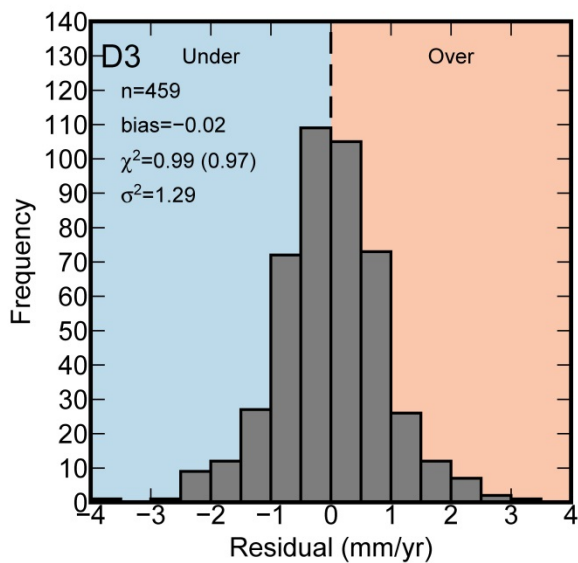
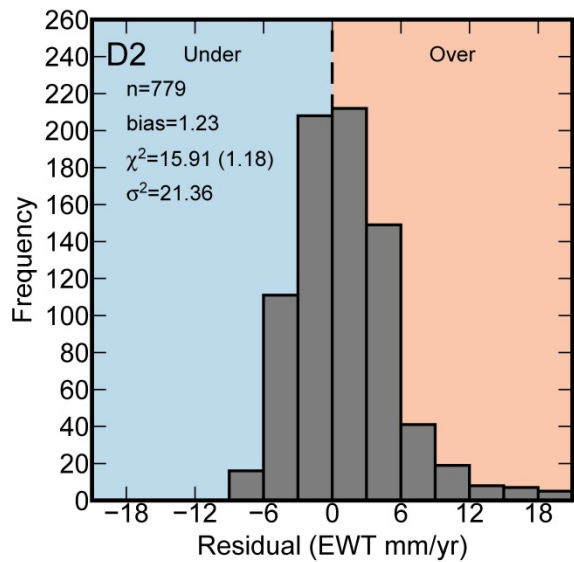
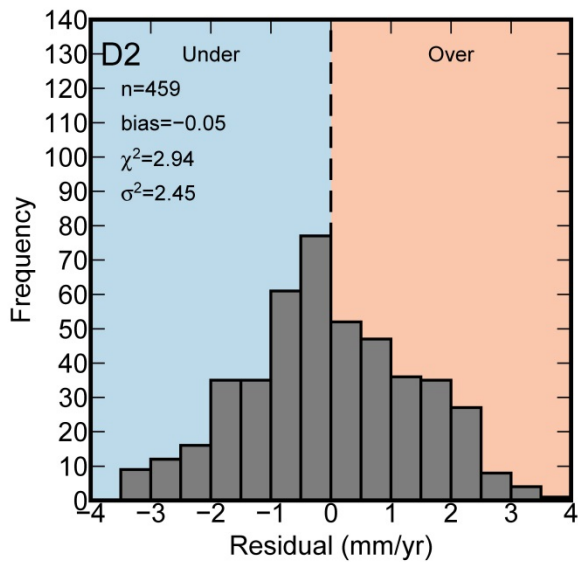
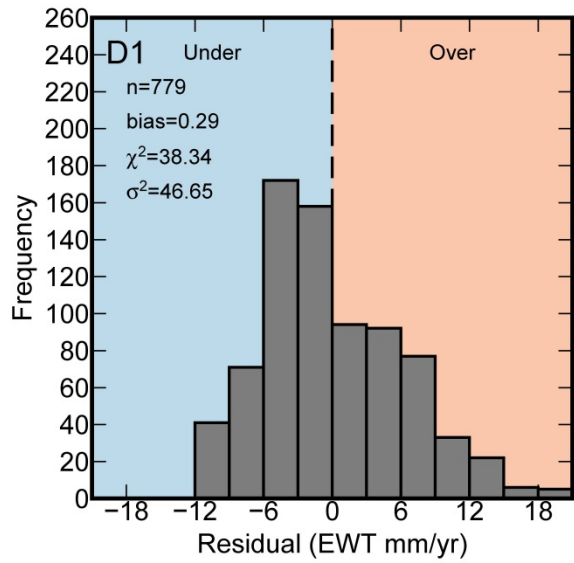
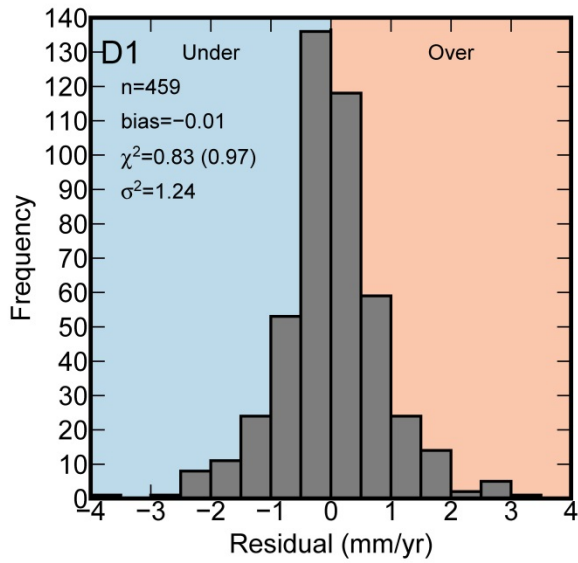
386



387

388 **Figure 8.** Spatial residuals for the D3 model for vertical motion (top) and gravity change (bottom). In
 389 top panel, triangles indicate model prediction is outside the 1σ uncertainty of the measurement, circles
 390 indicate model prediction is inside the 1σ uncertainty of the measurement.

391



393 **Figure 9.** Histogram of residuals for models D1-D3, for prediction of vertical motion (left) and gravity
394 change (right). Pink and blue shading indicate model overprediction and underprediction, respectively.
395 Where given, χ^2 values in brackets show the VCE-scaled χ^2 value.

396

397

398 3.3 Comparison of Vertical Motion Prediction to Other Models

399 We compare the vertical motion prediction of D1 to two other models. The first model is the forward
400 GIA model ICE-6G (Peltier et al. 2015) which is constrained by a global dataset of vertical land motion
401 measurements. The majority of these data are GPS measurements from the global solution of
402 JPL; within the study area of Scandinavia and northern Europe, additional measurements come from
403 the BIFROST GPS network as well as a small number of SLR, DORIS and VLBI measurements
404 (Argus et al. 2014, Peltier et al. 2015). The second model is the semi-empirical land uplift model
405 NKG2016LU (Vestøl et al. 2016) designed by several researchers in collaboration with the Nordic
406 Geodetic Commission (NKG). This model is constrained with GPS-measured vertical land motion
407 rates updated from the dataset of Kierulf et al. (2014), levelling measurements and GIA model
408 predictions and provides a semi-empirical estimate of total present-day vertical land motion.

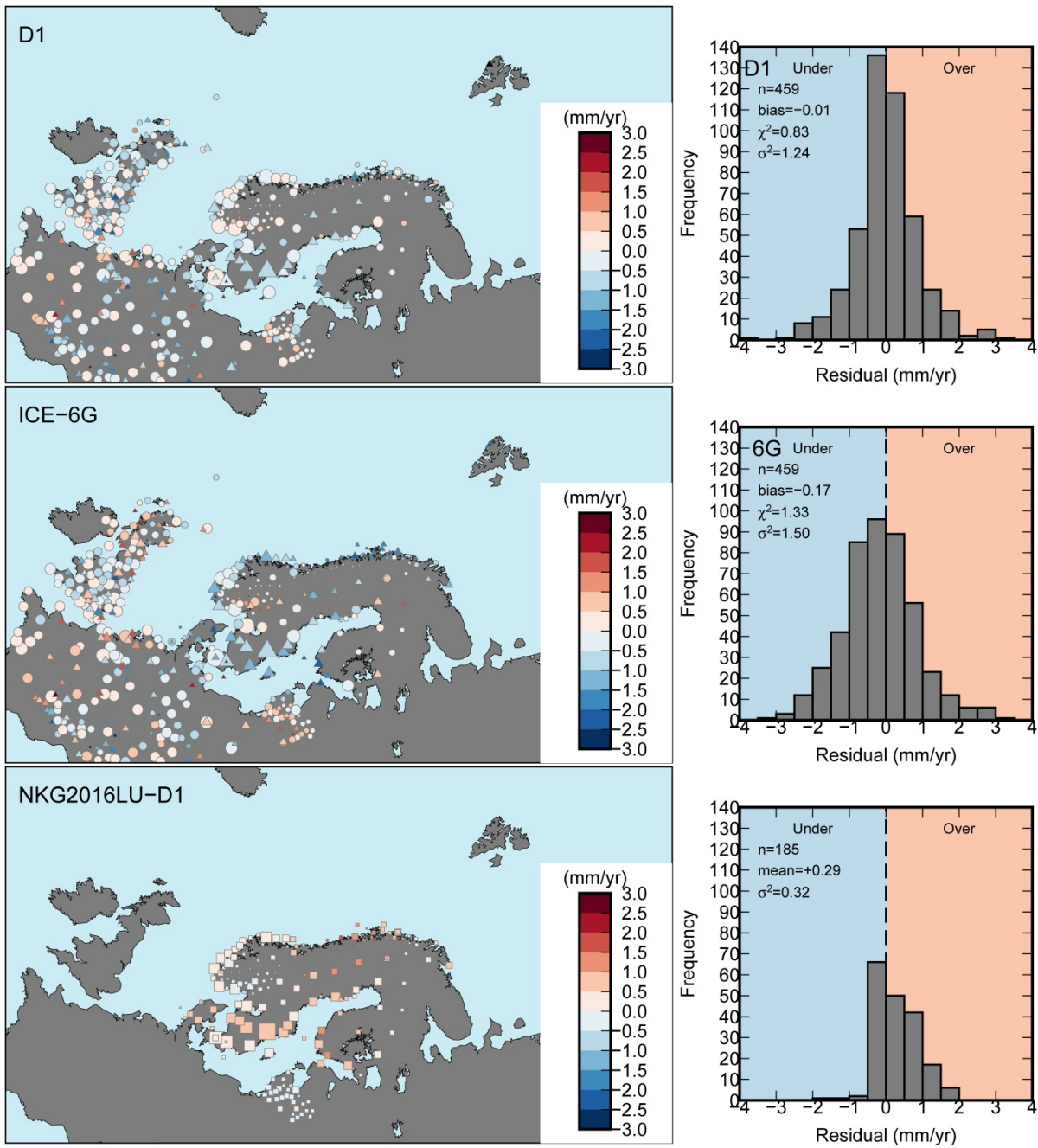
409

410 **Figure 10** compares the vertical land motion predictions of D1, ICE-6G and NKG2016LU. The ICE-6G
411 comparison is made relative to the vertical motion dataset presented in this paper, although as stated
412 above, it was constrained with a different variant of regional vertical land motion data. As well,
413 NKG2016LU predictions are available on a smaller grid and best fits data from Scandinavia and the
414 Baltic countries, thus, we limit our comparison with this model to north of 55°N (reducing the
415 comparison dataset from 459 to 185 sites).

416

417 With no significant bias and a χ^2 value of less than 1, the D1 model provides a good fit to the data. As
418 with the D3 model, the D1 model underpredicts vertical motion over the northern British Isles, and
419 appears also to overpredict vertical motion around the Netherlands. The ICE-6G model underpredicts
420 vertical motion at several sites in Scandinavia and has an overall χ^2 value of 1.33, somewhat higher
421 than that of D1. At station NYAL on Svalbard, both the D1 and ICE-6G models underpredict vertical

422 motion by more than 2 mm/yr, even after the applied corrections for present-day mass loss and
423 possible LIA uplift. When the NKG2016LU model is evaluated relative to the GPS data without an
424 elastic correction applied, the χ^2 value is less than 1, similar to D1. **Figure 10** shows the difference in
425 the prediction of vertical motion between NKG2016LU and D1. The former has consistently higher
426 predicted uplift rates over the study area, with an average difference of +0.3 mm/yr., which is primarily
427 the result of applying the elastic correction to the data used in the D1 model. D1 is therefore to the
428 extent that is possible, an estimate of the paleo GIA signal rather than the total uplift signal. That the
429 statistical fit to the data of both D1 and NKG2016LU is slightly better than the fit of the ICE-6G forward
430 model is expected due to the fundamental difference in model type: unlike ICE-6G, both of the semi-
431 empirical models explicitly incorporate the data into the prediction via formal inversion. Conversely, an
432 advantage of ICE-6G and other models of its type is the direct insight they offer into the space-time
433 evolution of the ice sheets, which cannot be inferred from a present-day empirical prediction alone.



434

435 **Figure 10.** Spatial (left) and binned (right) vertical motion residuals for D1 and ICE-6G and the
 436 difference between the NKG2016LU and D1 models. Triangles indicate model prediction is outside the
 437 1σ uncertainty of the measurement, circles indicate model prediction is inside the 1σ uncertainty of the
 438 measurement, squares show the difference between the two models (bottom left).

439

440 3.4 Tide Gauge Comparison

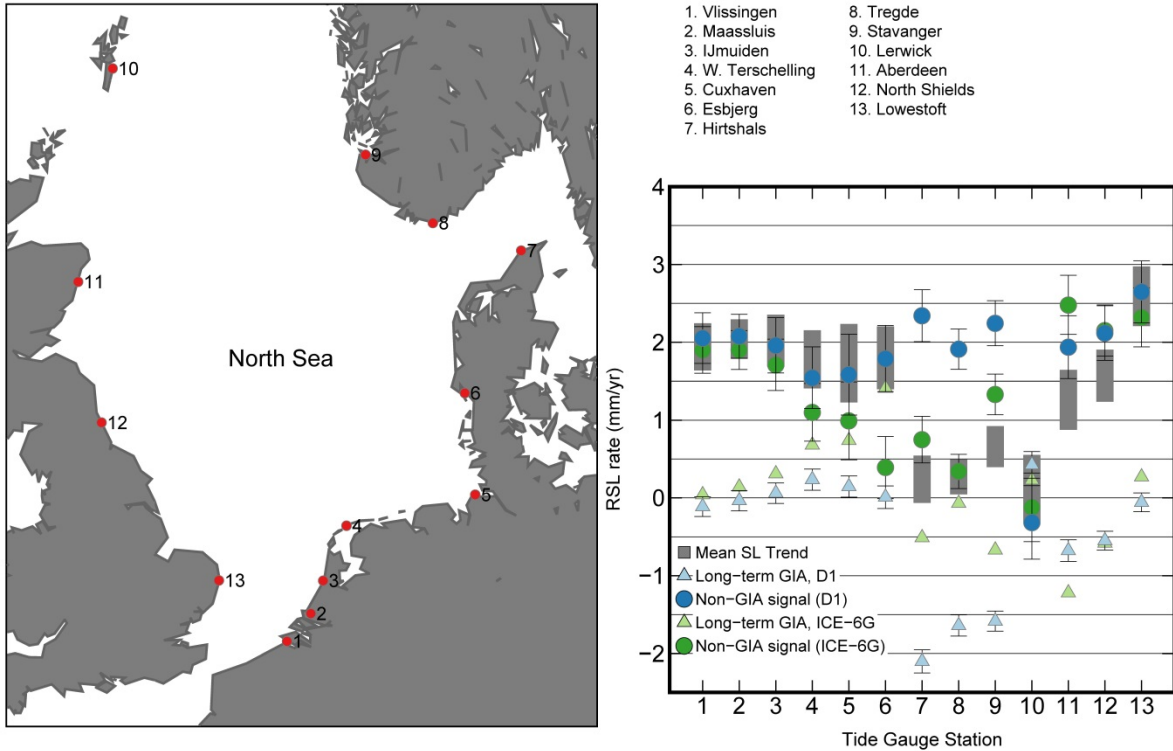
441 To assess the effect of GIA on regional sea-level change, we remove model D1's predictions of long-
 442 term GIA from mean sea-level trends at 13 tide gauge sites along the coast of the North Sea and 7
 443 tide gauge sites along the Norwegian coast (**Figures 11, 12**). The sea-level trends are taken from

444 Frederikse et al. (2016) who estimated the rates at Permanent Service for Mean Sea Level (PSMSL)
445 sites over the time interval 1958-2014. We also compare the effect of removing the modelled relative
446 sea-level rates of ICE-6G at the same PSMSL locations. For both the North Sea and the Norwegian
447 coastline, application of the D1 long-term sea-level trends to the total sea-level trends reduces the
448 interstation variability and infers a similar rate of non-GIA sea-level change (1.89 mm/yr and 1.84
449 mm/yr respectively).

450

451 *North Sea*

452 When corrected for the D1 long-term GIA trends, which are assumed to be linear over decadal time-
453 scales, the standard deviation of the trends decreases somewhat from 0.81 mm/yr to 0.71 mm/yr. The
454 D1 GIA correction is small at most sites, and at all sites except 7-9 (Hirtshals, Tregde and Stavanger),
455 the averaged sea-level trends appear dominated by processes other than long-term GIA (**Figure 11**).
456 At Hirtshals, Tregde and Stavanger, which are located nearest to the centre of the former FIS, the
457 predicted GIA-induced sea-level trend is more than twice the magnitude of the averaged sea-level
458 trend and removing the GIA signal shifts the original trend at these locations closer to the mean of the
459 13 locations. When the ICE-6G rates are removed from the sea-level trends, the interstation variability
460 and standard deviation (from 0.81 mm/yr to 0.83 mm/yr) are relatively unchanged. Regionally, the
461 average D1 GIA model trend is ~ -0.45 mm/yr for the North Sea which is larger in magnitude than the
462 ICE-6G GIA trend of ~ -0.06 mm/yr in the North Sea. This difference may in part be due to the influence
463 of the ANU ice sheet model in the prior model, which predicts stronger subsidence over the North Sea
464 than either ICE-5G or ICE-6G. Accordingly, removal of the GIA signal from all 13 locations changes
465 the North Sea mean sea-level trend from 1.39 mm/yr to 1.84 mm/yr for D1 and to 1.33 mm/yr for ICE-
466 6G. Station Lerwick is particularly discrepant; removing it from the comparison decreases the standard
467 deviation of the non-GIA rates to 0.45 mm/yr for D1 and 0.75 mm/yr for ICE-6G. The variability at
468 Lerwick is insensitive to application of the relatively small and linear GIA correction for this region and
469 cannot be explained by GIA-induced sea-level change. Conversely, the variability in sea-level trends
470 in the northeast North Sea, near the former FIS, is easily attributed to GIA for model D1.



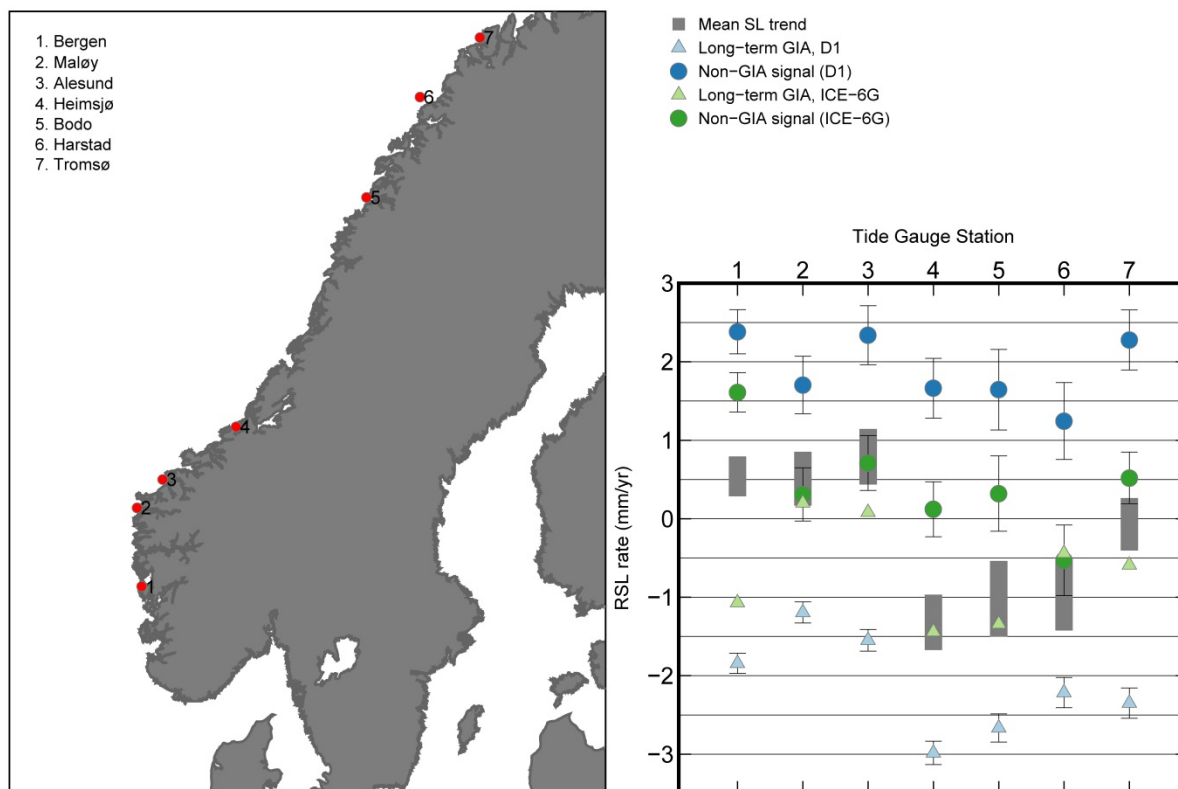
471 **Figure 11.** Comparison of mean total, long-term GIA and non-GIA sea-level trends (grey boxes,
 472 triangles, circles) for 13 tide gauge stations in the North Sea. Long-term GIA trends are from model D1
 473 and ICE-6G, mean sea-level trends are from Frederikse et al. (2016).
 474

475

476 *Norwegian Coast*

477 The average sea-level trend for the 7 sites along the Norwegian coast is -0.22 mm/yr with a standard
 478 deviation of 0.87 mm/yr. Removal of the D1 long-term GIA trends increases the average sea-level
 479 trend to 1.89 mm/yr and reduces the interstation variability (0.44 mm/yr standard deviation) (**Figure**
 480 **12**). The same is true for ICE-6G, although the magnitude of the changes are smaller (0.44 mm/yr
 481 mean, 0.65 mm/yr standard deviation). This difference is owing to the relatively larger average GIA-
 482 related relative sea-level change for D1 (-2.11 mm/yr) compared to ICE-6G (-0.66 mm/yr). The
 483 gradient of predicted GIA changes across the Norwegian coastline is steep, so the results may also be

484 sensitive to the resolution of the GIA models.



485
486 **Figure 12.** Same as caption for Figure 11, except for tide gauge locations along the Norwegian
487 coastline.

488
489 **4. Conclusion**

490 We generate a data-driven prediction of the long-term GIA response at present-day in Scandinavia,
491 northern Europe and the Barents Sea through the simultaneous inversion of GPS-measured vertical
492 motion rates, GRACE-measured gravity change rates, and a *priori* GIA model information. In models
493 D1-D3, we predict GIA motions for the inversion of the vertical motion data, the gravity data, and both
494 datasets. In both the χ^2 and RMS sense, the vertical motion data alone have the poorest ability to
495 predict gravity change, and vice versa. Predictions of the D3 model provide the best overall fit to both
496 datasets.

497
498 In general, prediction of the gravity signal is problematic, with larger χ^2 values than those obtained for
499 the vertical motion prediction. The poorer prediction of gravity change is in part due to the uncertainty

500 of the present-day mass loss effect in the Barents Sea region. The mass loss signal estimated by
501 GRACE over Svalbard and the Russian Arctic is significantly smaller than estimates obtained from
502 satellite altimetry. This difference may be the result of signal loss in the GRACE data from application
503 of the Wiener filter or may also indicate that there is a non-zero component of ongoing glacial isostatic
504 adjustment from the LIA.

505

506 The vertical motion signal is overall better predicted than the gravity signal. Both the D1 and D3
507 models have χ^2 values of ≤ 1 and predict rates of vertical motion that are within the 1σ uncertainty of
508 the observations throughout most of the study area. Regions of misfit persist in Scotland and around
509 the Netherlands, where the model underpredicts and overpredicts rates of vertical motion,
510 respectively. The misfit in Scotland may be partly due to both positive and negative rates of vertical
511 motion that are present in the data over relatively short distances. Further analysis and filtering of the
512 GPS dataset may be useful in this region. In the Netherlands, Kooi et al. (1998) found that present-day
513 subsidence from sediment compaction as well as tectonic movements may contribute significantly to
514 vertical land motion; correction for these effects may serve to reduce some of the residuals in this
515 region. There may also be significant neotectonic movements in central Norway (Kierulf et al. 2014),
516 which may explain some of the misfits that remain mainly along the central Norwegian coastline
517 **(Figure 8)**.

518

519 The prediction of vertical land motion has a small but non-negligible sensitivity to the application of an
520 elastic correction. The elastic correction applied in this study is between 0.2-0.5 mm/yr; the largest
521 contribution comes from mass loss of the Greenland Ice Sheet which yields regional uplift with a
522 southeastward decreasing gradient. When the model predictions from another semi-empirical model of
523 vertical motion, NKG2016LU, are compared to D1, a small but relatively uniform difference of +0.3
524 mm/yr is present in the model predictions over Scandinavia. Both NKG2016LU and D1 (and D3) have
525 vertical motion χ^2 values ≤ 1 over their respective study areas. However, while the magnitude of the
526 difference is smaller than the observational uncertainty on many of the measurements, it is generally
527 larger than the estimated *a posteriori* model uncertainty. Also, because only anthropogenic

528 hydrological signals (and not natural hydrological signals) were included in the elastic correction, it is
529 possible that the applied elastic correction is conservative in this region.

530

531 Therefore, the presence of such a difference in the vertical motion prediction suggests that while long-
532 term GIA is the dominant contributor to vertical motion in central Scandinavia, that it is still worthwhile
533 to correct GPS land motion rates for present-day elastic signals, so long as these signals are
534 adequately approximated (e.g., Riva et al. 2017). This conclusion however highlights a fundamental
535 assumption that underpins the data-driven methodology: that the input data can be adequately
536 'cleaned' for processes not arising from long-term GIA. Even with applied corrections for hydrology
537 and contemporary ice mass loss, this assumption may not always be adequate, especially in regions
538 where model misfits relative to the data are spatially coherent. Thus, the success of data-driven GIA
539 predictions are evaluated by two criteria: i) the estimation of realistic *a posteriori* uncertainties that are
540 smaller than those associated with *a priori* knowledge and measurement uncertainty, and ii) the ability
541 of the final model to provide a good fit to the data. The vertical motion predictions of models D1 and
542 D3 satisfy both criteria for most of the study area and thus can provide a useful tool with which to
543 separate long-term GIA signals from shorter-term forcing.

544

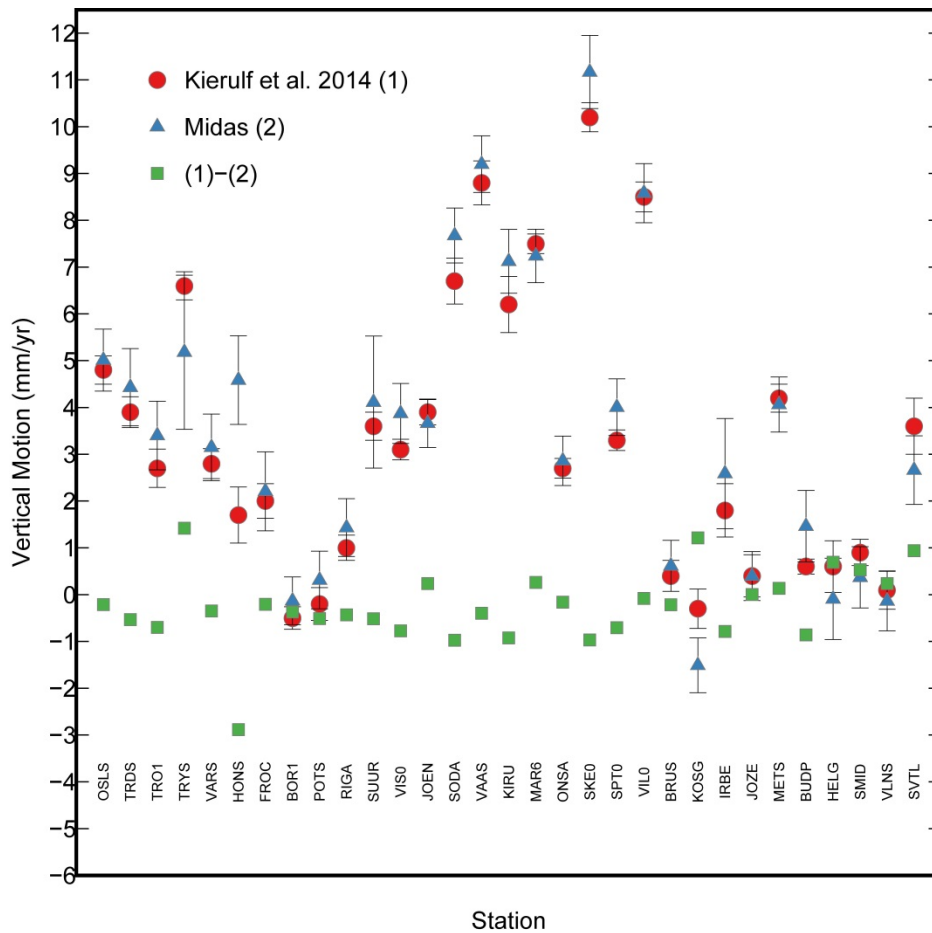
545 **Data Availability**

546

547 Gridded vertical land motion predictions for the D1 model are available at the 4TU Centre for
548 Research Data repository, <https://data.4tu.nl/>, doi:10.4121/uuid:4a495bbc-0478-483a-baef-
549 19ff34103dd2.

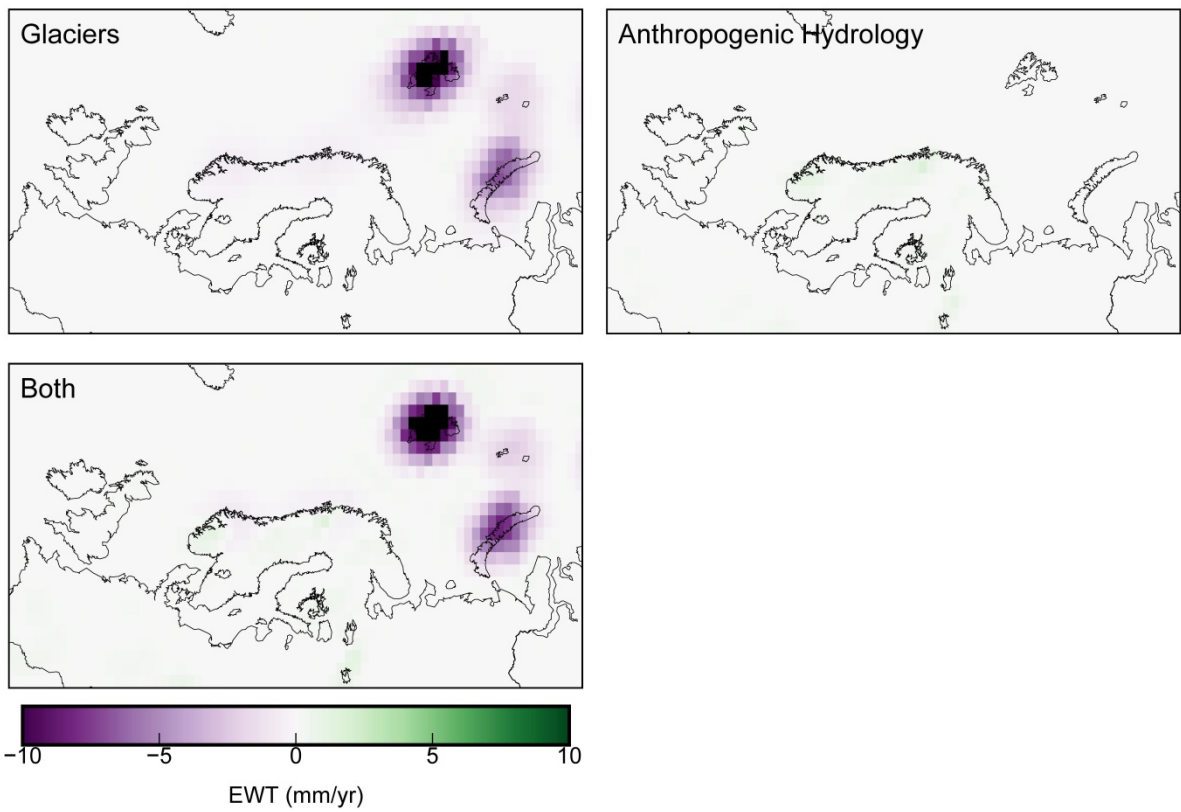
550 **Appendix**

551 The 31 GPS measurements that are common to the Kierulf et al. (2014) and Nevada Geodetic
 552 Laboratory (Blewitt et al. 2016) datasets are shown in **Figure A1**. The individual anthropogenic
 553 hydrology and glacial mass change contributions to the GRACE correction are shown in **Figure A2**.



554

555 **Figure A1.** Vertical land motion measurements at 31 sites common to both datasets used in this
 556 study.



557

558 **Figure A2.** Individual and combined contributions to the correction applied to the GRACE data
 559 (combined is the same as **Figure 2c**).

560

561 **Acknowledgements**

562 We would like to thank Anthony Purcell for providing the ANU ice sheet model for Europe and the
563 British Isles, Yoshihide Wada for making the PCR-GLOBWB hydrology model available, and Bert
564 Wouters for providing altimetry estimates of recent mass loss for Svalbard and the Russian Arctic. We
565 also thank two anonymous reviewers for comments that improved the manuscript. This work is part of
566 the project for a Multi-Scale Sea-Level model (MuSSeL), funded by the Netherlands Organization for
567 Scientific Research, VIDI Grant No. 864.12.012.

568 **References**

- 569 Altamimi, Z., Collillieux, X., and Métivier, L., 2011. ITRF2008: an improved solution of the international
570 terrestrial reference frame. *Journal of Geodesy* 85, 457–473, doi:10.1007/s00190-011-0444-
571 4.
- 572 Argus, D.F., Peltier, W.R., Drummond, R., and Moore, A.W., 2014. The Antarctica component of
573 postglacial rebound model ICE-6G_C (VM5a) based on GPS positioning, exposure age
574 dating of ice thicknesses, and relative sea level histories. *Geophysical Journal International*
575 198, 537–563, doi:10.1093/gji/ggu140.
- 576 Auriac, A., Whitehouse, P.L., Bentley, M.J., Patton, H., Lloyd, J.M., and Hubbard, A., 2016. Glacial
577 isostatic adjustment associated with the Barents Sea ice sheet: A modelling inter-
578 comparison. *Quaternary Science Reviews* 147, 122-135,
579 doi:10.1016/j.quascirev.2016.02.011.
- 580
581 Blewitt, G., Kreemer, C., Hammond, W.C., and Gazeaux, J., 2016. MIDAS robust trend estimator for
582 accurate GPS station velocities without step detection. *Journal of Geophysical Research -*
583 *Solid Earth* 121, doi:10.1002/2015JB012552.
- 584 Bradley, S.L., Milne, G.A., Shennan, I., and Edwards, R., 2011. An improved glacial isostatic
585 adjustment model for the British Isles. *Journal of Quaternary Science* 26, 541-552,
586 doi:10.1002/jqs.1481.
- 587 Chao, B.F., Wu, Y.H., and Li, Y.S., 2008. Impact of artificial reservoir water impoundment on global
588 sea level. *Science* 320, 212–214, doi:10.1126/science.1154580.
- 589
590 Cheng, M.K., Tapley, B.D., and Ries, J.C., 2013. Deceleration in the Earth's oblateness. *Journal of*
591 *Geophysical Research* 118, 740-747, doi:10.1002/jgrb.50058.
- 592
593 Dziewonski, A.M., and Anderson, D.L., 1981. Preliminary reference Earth model. *Physics of the Earth*
594 *and Planetary Interiors* 25, 297-356.
- 595
596 Farrell, W.E., 1972. Deformation of the Earth by surface loads. *Reviews of Geophysics and Space*
597 *Physics* 10, 761-797.
- 598
599 Frederikse, T., Riva, R., Kleinherenbrink, M., Wada, Y., van den Broeke, M., and Marzeion, B., 2016.
600 Closing the sea level budget on a regional scale: Trends and variability on the Northwestern
601 European continental shelf. *Geophysical Research Letters* 43, doi:10.1002/2016GL070750.
- 602
603 Gardner, A.S., Moholdt, G., Cogley, J.G., Wouters, B., Arendt, A.A., Wahr, J., Berthier, E., Hock, R.,
604 Pfeffer, W.T., Kaser, G., Ligtenberg, S.R.M., Bolch, T., Sharp, M.J., Hagen, J.O., van den
605 Broeke, M.R., and Paul, F., 2013. A reconciled estimate of glacier contributions to sea level
606 rise: 2003 to 2009. *Science* 340, 852-857, doi:10.1126/science.1234532.
- 607
608 Gunter, B.C., Didova, O., Riva, R.E.M., Ligtenberg, S.R.M., Lenaerts, J.T.M., King, M.A., van den
609 Broeke, M.R., and Urban, T., 2014. Empirical estimation of present-day Antarctic glacial
610 isostatic adjustment and ice mass change. *The Cryosphere* 8, 743–760, doi:10.5194/tc-8-
611 743-2014.
- 612
613 Herring, T., King, R., and McClusky, S., 2011. Introduction to GAMIT/GLOBK release 10.4, Technical
614 Report, Massachusetts Institute of Technology, Cambridge, USA.
- 615
616 Hill, E.M., Davis, J.L., Tamisiea, M.E., and Lidberg, M., 2010. Combination of geodetic observations
617 and models for glacial isostatic adjustment fields in Fennoscandia. *Journal of Geophysical*
618 *Research* 115, doi:10.1029/2009JB006967.
- 619

- 620 Hughes, A.L.C., Gyllencreutz, R., Lohne, Ø.S., Mangerud, J., and Svendsen, J.I., 2016. The last
621 Eurasian ice sheets – a chronological database and time-slice reconstruction, DATED-1.
622 *Boreas* 45, 1–45, doi:10.1111/bor.12142.
623
- 624 Jin, S., Zhang, T.Y., and Zou, F., 2016. Glacial density and GIA in Alaska estimated from ICESat,
625 GPS and GRACE measurements. *Journal of Geophysical Research* 122,
626 doi:10.1002/2016JF003926.
627
- 628 Kierulf, H.P., Steffen, H., Simpson, M.J.R., Lidberg, M., Wu, P., and Wang, H. 2014. A GPS velocity
629 field for Fennoscandia and a consistent comparison to glacial isostatic adjustment models.
630 *Journal of Geophysical Research* 119, 6613–6629, doi:10.1002/2013JB010889.
- 631 Klees, R., Revtova, E.A., Gunter, B.C., Ditmar, P., Oudman, E., Winsemius, H.C., and Savenije,
632 H.H.G., 2008. The design of an optimal filter for monthly GRACE gravity models.
633 *Geophysical Journal International* 175, 417–432, doi:10.1111/j.1365-246X.2008.03922.x.
634
- 635 Kooi, H., Johnston, P., Lambeck, K., Smither, C., Molendijk, R., 1998. Geological causes of recent
636 (~100 yr) vertical land movement in the Netherlands. *Tectonophysics* 299, 297–316.
637
- 638 Kuchar, J., Milne, G., Hubbard, A., Patton, H., Bradley, S., Shennan, I., and Edwards, R., 2012.
639 Evaluation of a numerical model of the British–Irish ice sheet using relative sea-level data:
640 implications for the interpretation of trimline observations. *Journal of Quaternary Science* 27,
641 597–605, doi:10.1002/jqs.2552.
- 642 Lambeck, K., Smither, C., and Johnston, P., 1998. Sea-level change, glacial rebound and mantle
643 viscosity for northern Europe. *Geophysical Journal International* 177, 102-144.
644
- 645 Lambeck, K., Purcell, A., Zhao, J. and Svensson, N.-O., 2010. The Scandinavian ice sheet: from MIS
646 4 to the end of the last glacial maximum. *Boreas* 39, 410–435, doi:10.1111/j.1502-
647 3885.2010.00140.x.
648
- 649 Lidberg, M., Johansson, J.M., Scherneck, H.-G., and Milne, G.A., 2010. Recent results based on
650 continuous GPS observations of the GIA process in Fennoscandia from BIFROST. *Journal*
651 *of Geodynamics* 50, 8–18, doi:10.1016/j.jog.2009.11.010.
652
- 653 Marzeion, B., Jarosch, A.H., and Hofer, M., 2012. Past and future sea-level change from the surface
654 mass balance of glaciers. *The Cryosphere* 6, 1295–1322, doi:10.5194/tc-6-1295-2012.
655
- 656 Marzeion, B., Leclercq, P.W., Cogley, J.G., and Jarosch, A.H., 2015. Brief Communication: Global
657 reconstructions of glacier mass change during the 20th century are consistent. *The*
658 *Cryosphere* 9, 2399–2404, doi:10.5194/tc-9-2399-2015.
659
- 660 Mémin, A., Spada, G., Boy, J.-P., Rogister, Y., and Hinderer, J., 2014. Decadal geodetic variations in
661 Ny-Ålesund (Svalbard): role of past and present ice-mass changes. *Geophysical Journal*
662 *International* 198, 285-297, doi:10.1093/gji/ggu134.
663
- 664 Milne, G.A., Davis, J.L, Mitrovica, J.X., Scherneck, H.-G., Johansson, J.M., Vermeer, M., and Koivula,
665 H., 2001. Space-geodetic constraints on glacial isostatic adjustment in Fennoscandia.
666 *Science* 291, 2381-2385.
667
- 668 Müller, J., Naeimi, M., Gitlein, O., Timmen, L., and Denker, H., 2012. A land uplift model in
669 Fennoscandia combining GRACE and absolute gravimetry data. *Physics and Chemistry of*
670 *the Earth* 53–54, 54–60, doi:10.1016/j.pce.2010.12.006.
671
- 672 Noël, B., van de Berg, W.J., van Meijgaard, E., Munneke, P.K., van de Wal, R.S.W., and van den
673 Broeke, M.R., 2015. Evaluation of the updated regional climate model RACMO2.3: Summer
674 snowfall impact on the Greenland Ice Sheet, *The Cryosphere* 9, 1831–1844, doi:10.5194/tc-
675 9-1831-2015.
676
- 677 Patton, H., Hubbard, A., Andreassen, K., Auriac, A., Whitehouse, P.L., Stroeven, A.P., Shackleton, C.,
678 Winsborrow, M., Heyman, J., and Hall, A.M., 2017. Deglaciation of the Eurasian ice sheet
679 complex. *Quaternary Science Reviews* 169, 148-172, doi:10.1016/j.quascirev.2017.05.019.

680
681 Peltier, W.R., Andrews, J.T., 1976. Glacial-isostatic adjustment I – The forward problem. *Geophysical*
682 *Journal of the Royal Astronomical Society* 46, 605–646.
683
684 Peltier, W.R., 1998. Postglacial variations in the level of the sea: implications for climate dynamics and
685 solid Earth geophysics. *Reviews of Geophysics* 36, 603-689.
686
687 Peltier, W.R., 2004. Global glacial isostasy and the surface of the ice-age Earth: The ICE-5G (VM2)
688 model and GRACE. *Annual Reviews of Earth and Planetary Sciences* 32, 111–149,
689 doi:10.1146/annurev.earth.32.082503.144359.
690
691 Peltier, W.R., Argus, D.F., and Drummond, R., 2015. Space geodesy constrains ice age terminal
692 deglaciation: The global ICE-6G_C (VM5a) model. *Journal of Geophysical Research* 119,
693 doi:10.1002/2014JB011176.
694
695 Riva, R.E.M., Gunter, B.C., Urban, T.J., Vermeersen, B.L.A., Lindenbergh, R.C., Helsen, M.M.,
696 Bamber, J.L., van de Wal, R.S.W., van den Broeke, M.R., and Schutz, B.E., 2009. Glacial
697 isostatic adjustment over Antarctica from combined ICESat and GRACE satellite data. *Earth*
698 *and Planetary Science Letters* 288 516–523, doi:10.1016/j.epsl.2009.10.013.
699
700 Riva, R.E.M., Frederikse, T., King, M.A., Marzeion, B., and van den Broeke, M.R., 2017. Brief
701 Communication: The global signature of post-1900 land ice wastage on vertical land motion.
702 *The Cryosphere* 11, 1327–1332, doi:10.5194/tc-11-1327-2017.
703
704 Root, B.C., Tarasov, L., and van der Wal, W., 2015. GRACE gravity observations constrain
705 Weichselian ice thickness in the Barents Sea. *Geophysical Research Letters* 42, 3313–3320,
706 doi:10.1002/2015GL063769.
707
708 Sasgen, I., Klemann, V., and Martinec, Z., 2012. Towards the inversion of GRACE gravity fields for
709 present-day ice-mass changes and glacial-isostatic adjustment in North America and
710 Greenland. *Journal of Geodynamics* 59–60, 49–63, doi:10.1016/j.jog.2012.03.004.
711
712 Schmidt, P., Lund, B., Näslund, J.-O., and Fastook, J., 2014. Comparing a thermo-mechanical
713 Weichselian Ice Sheet reconstruction to reconstructions based on the sea level equation:
714 aspects of ice configurations and glacial isostatic adjustment. *Solid Earth* 5, 371–388,
715 doi:10.5194/se-5-371-2014.
716
717 Schrama, E.J.O., Wouters, B., and Rietbroek, R., 2014. A mascon approach to assess ice sheet and
718 glacier mass balances and their uncertainties from GRACE data. *Journal of Geophysical*
719 *Research* 119, 6048–6066, doi:10.1002/2013JB010923.
720
721 Shepherd, A. *et al.*, 2012. A reconciled estimate of ice-sheet mass balance, *Science* 338, 1183–1189,
722 doi:10.1126/science.1228102.
723
724 Siemes, C., Ditmar, P., Riva, R.E.M., Slobbe, D.C., Liu, X.L., and Hashemi Farahani, H., 2013.
725 Estimation of mass change trends in the Earth’s system on the basis of GRACE satellite
726 data, with application to Greenland. *Journal of Geodesy* 87, 69-87, doi:10.1007/s00190-012-
727 0580-5.

728 Simon, K.M., James, T.S., and Dyke, A.S., 2015. A new glacial isostatic adjustment model of the
729 Innuitian Ice Sheet, Arctic Canada. *Quaternary Science Reviews* 119, 11–21,
730 doi:10.1016/j.quascirev.2015.04.007.

731 Simon, K.M., James, T.S., Henton, J.A., and Dyke, A.S., 2016. A glacial isostatic adjustment model for
732 the central and northern Laurentide Ice Sheet based on relative sea-level and GPS
733 measurements. *Geophysical Journal International* 205, 1618-1636, doi:10.1093/gji/ggw103.
734
735 Simon, K.M., Riva, R.E.M., Kleinherenbrink, M., and Tangdamrongsub, N., 2017. A data-driven model
736 for constraint of present-day glacial isostatic adjustment in North America. *Earth and*
737 *Planetary Science Letters* 474, 322-333, doi:10.1016/j.epsl.2017.06.046.

738 Steffen, H., Wu, P., Wang, H., 2010. Determination of the Earth's structure in Fennoscandia from
739 GRACE and implications for the optimal post-processing of GRACE data. *Geophysical*
740 *Journal International* 182, 1295–1310, doi:10.1111/j.1365-246X.2010.04718.x.
741

742 Steffen, H., and Wu, P., 2011. Glacial isostatic adjustment in Fennoscandia - a review of data and
743 modeling. *Journal of Geodynamics* 52, 169–204, doi:10.1016/j.jog.2011.03.002.
744

745 Tamisiea, M.E., 2011. Ongoing glacial isostatic contributions to observations of sea level change.
746 *Geophysical Journal International* 186, 1036-1044, doi:10.1111/j.1365-246X.2011.05116.x.
747

748 van den Broeke, M. R., Enderlin, E.M., Howat, I.M., Munneke, P.K., Noël, B.P.Y., van de Berg, W.J.,
749 van Meijgaard, E., and Wouters, B., 2016. On the recent contribution of the Greenland ice
750 sheet to sea level change, *Cryosphere* 10, 1933–1946, doi:10.5194/tc-10-1933-2016.
751

752 van Wessem, J.M., Ligtenberg, S.R.M., Reijmer, C.H., van de Berg, W.J., van den Broeke, M.R.,
753 Barrand, N.E., Thomas, E.R., Turner, J., Wuite, J., Scambos, T.A., and van Meijgaard, E.,
754 2016. The modelled surface mass balance of the Antarctic Peninsula at 5.5 km horizontal
755 resolution. *The Cryosphere* 10, 271–285, doi:10.5194/tc-10-271-2016.
756

757 Vestøl, O., Ågren, J., Steffen, H., Kierulf, H., Lidberg, M., Oja, T., Rüdja, A., Kall, T., Saaranen, V.,
758 Engsager, K., Jepsen, C., Liepins, I., Paršeliūnas, E., and Tarasov, L., 2016. NKG2016LU,
759 an improved postglacial land uplift model over the Nordic-Baltic region. *Nordic Geodetic*
760 *Commission (NKG) Working Group of Geoid and Height Systems*,
761 <http://www.lantmateriet.se/sv/Kartor-och-geografisk-information/GPS-och-geodetiskmatning/>.
762

763 Wada, Y., Wisser, D., and Bierkens, M.F.P., 2014. Global modeling of withdrawal, allocation and
764 consumptive use of surface water and groundwater resources. *Earth System Dynamics* 5,
765 15–40, doi:10.5194/esd-5-15-2014.
766

767 Wouters, B., 2016. Personal communication.
768

769 Wu, P., and Peltier, W.R., 1982. Viscous gravitational relaxation. *Geophysical Journal of the Royal*
770 *Astronomical Society* 70, 435-485.
771

772 Zhao, S., Lambeck, K., and Lidberg, M., 2012. Lithosphere thickness and mantle viscosity inverted
773 from GPS-derived deformation rates in Fennoscandia. *Geophysical Journal International*
774 190, 278-292, doi:10.1111/j.1365-246X.2012.05454.x.